AUT Journal of Mechanical Engineering

AUT J. Mech. Eng., 7(2) (2023) 91-116
DOI: 10.22060/ajme.2023.21259.6031

A modified biogas-driven combined cooling and power system based on open and close Brayton cycles

Amir Hamazeh Farajollahi[1], Mohsen Rostami[1], Mohammad Reza Salimi[2,*], Farzaneh Behnam[3]

[1] Department of Aerospace Engineering, Imam Ali University, Tehran, Iran
[2] Aerospace Research Institute, Tehran, Iran
[3] Department of Mechanical Engineering, Faculty of Engineering, University of Mohaghegh Ardabili, Ardabil, Iran

ABSTRACT: A novel method of a biogas-driven cogeneration system for electricity and cooling with recovering liquefied natural gas heat sink is introduced in this study. The proposed system consists of an open loop Brayton cycle or gas turbine cycle fed by biogas, a close loop Brayton cycle, a liquefied natural gas open power generation cycle, and a dual-stage combined cooling and power unit composed of an organic Rankine cycle integrated with an ejector refrigeration cycle. The superiority of the system over previous models is demonstrated from the thermodynamic and economic points of view. In addition, a multi-criteria optimization of the proposed set-up is conducted regarding crucial decision variables, energy and exergy metrics, and unit overall product cost as objective functions. It is deduced that gas turbine 1 inlet temperature is the most influential decision variable affecting the objective functions. From the optimization, it is discovered that the developed unit can generate cooling and net electricity of 424.1 kW and 1,864 kW, correspondingly, resulting in energetic efficiency of 80.4%, exergetic efficiency of 41.24%, and unit cost of 10.07 $/GJ. The performance of the biogas-fueled combined system can be improved by 71.17% in the form of energy efficiency at the optimum scenario. Among all elements available in the developed cogeneration system, the combustion chamber has the highest contribution to the overall exergy destruction rate, followed by the condenser.

Review History:

Received: Apr. 01, 2022
Revised: Aug, 28, 2022
Accepted: Sep. 16, 2022
Available Online: Jun. 30, 2023

Keywords:

Biogas
Thermodynamic analysis
Economic analysis
Genetic algorithm
Cogeneration

1- Introduction

The utilization of renewable energy in integrated energy systems is boosted in recent years due to the policy of limiting the use of fossil fuels worldwide. Here, the waste heat of energy systems driven by biogas can be utilized for augmenting the performance of corresponding systems and decreasing the greenhouse gas footprint. Ghaebi et al. [1] utilized waste heat of a biogas steam reforming (BSR) system for electricity generation using an organic Rankine cycle (ORC) by using R600 as the working fluid. Optimum mode outlined that the system's critical parameters like steam/carbon ratio and carbon dioxide (CO_2)/methane (CH_4) ratio should be set at 2.99 and 0.502, respectively. Zareh et al. [2] devised a combined heat and power (CHP) system and outlined its exergoeconomic and thermodynamic relations when natural gas (NG) and biogas were used as inlet fuels. They concluded that the combustion chamber and anaerobic were two major contributor elements to the total irreversibility of the biogas scenario. The authors also deduced that the energetic performance factor of the unit increased from 46.94% to 50.64% and overall product cost (OPC) decreases from 98.71 $/MWh to 66.7 $/MWh when NG was utilized instead of biogas. Amiri et al. [3] developed a reliable optimization model for a biogas-driven CHP system in Sweden and discovered that CO_2 emission decreased by 21,000 ton/year when the proposed model was used instead of the conventional coal-fired power plant. Zeng et al. [4] employed a porous media burner in the combustor of a CHP system with non-catalytic fuel to guarantee a high-temperature and stable reformed syngas for a biogas-fueled solid oxide fuel cell (SOFC) to increase the starting time of the unit. The experimental results indicated that a reforming efficiency of 42.3% was achievable. Jabari et al. [5] designed a combined cooling and power (CCP) system using a biogas-driven gas turbine (GT) cycle for a hotel in Iran. The authors used a mixed integer nonlinear program to minimize the base value of the calculated OPC by reducing the power utilization of the set-up. Leonzio [6] designed and analyzed a biogas-driven trigeneration application using two heat pumps, a steam Rankine cycle power plant, and a heat recovery plant. This system produced 925 kW electricity, 473 kW cooling load, and 2523 kW thermal load respecting a biogas supply of 3280 kW, and reported a primary energy rate (PER) of 1.04. As a result of such a simulation, the designed unit decreased CO_2 emission by 40% and increased electricity output by 28%. Sevinchan et al. [7] employed a Brayton cycle, an ORC, a two-stage biomass digester, a water separator, a single-effect absorption cooling system (ACS), and a heat recovery unit for multi-generation. The devised unit produced a cooling load of 87.54 kW, electricity of 1078 kW, fresh water of 40 kg/day,

*Corresponding author's email: mohammadsalimi@ari.ac.ir

and a heating load of 198 kW. Besides, its overall first- and second-law efficiencies were found at 72.5% and 30.44%, correspondingly. Based on a BSR, Rostamzadeh et al. [8, 9] recommended the use of biogas hybridized with geothermal for polygeneration purposes and demonstrated the viability of their layout in from the economic, thermodynamic, and environmental viewpoints. They demonstrated that reducing the CO_2/CH_4 molar ratio or increasing the steam/carbon ratio increased the energetic performance of the whole set-up. Su et al. [10] transformed biogas into syngas via reforming reaction and then utilized solar energy to launch a combined cooling, heating, and power (CCHP) system. They outlined a higher operating performance of 5.41% for the hybrid solar-biogas CCHP system compared to the reference system. In a recent study, Liang et al. [11] optimized the performance of a novel solar-driven supercritical Brayton cycle (SBC) in terms of thermodynamics and ignored economic and environmental considerations during their optimization. In another study carried out by Ochoa et al. [12], the performance of a SBC coupled with an ORC was enhanced only in terms of thermodynamics through optimization; hence, accounting environment index (EI) and unit cost was ignored during the optimization. In another similar work, Yang et al. [13] included economic metric in multi-criteria optimization of a CCHP system based on the SBC, but they also excluded EI in their multi-objective optimization scheme.

Over the last years, several studies in biogas-driven integrated energy systems have been carried out to increase the performance of the topping system (i.e., the GT cycle), while producing several different energy products. Due to the promising potential of the biogas process for multi-production at large-scale capacities, its range of application can be modified to have more yields. Although some of these aims are achieved through previous studies, many investigations still are required to increase the value of the previously reported performance. For instance, in Ref. [14], the performance of the biogas-fueled GT cycle is improved by employing a modified ORC, and the superiority of the devised integrated power system was demonstrated in terms of thermodynamics and thermoeconomics. Although an ORC has more simpler structure and hence is more reliable, it should be stated that using organic refrigerant is still a dilemma in terms of flammability and toxicity. In addition, there is a relatively huge temperature mismatch between the exhaust gas and organic fluid at high exhaust gas temperatures, in which this negative point can be addressed by using a CLBC between the GT cycle and the proposed CCP system. In our previous studies, we have used waste thermal energy of the GT cycle via only one vapor generator for an ORC-based CCP system [15] or for the trigeneration of cooling, power, and freshwater [16]. However, in this study, in addition to the employment of the CLBC, a two-stage cooling/power cogeneration system based on ORC and ejector refrigeration cycle (ERC) is used. Through this study, it will be shown that using a power system working at high operating temperatures like a CLBC for waste heat recovery of the GT is much better than employing an ORC-based integrated system directly after the GT cycle. In fact, previously proposed systems like those presented in Refs. [14-16] suffers from a high exergy destruction due to low exergy efficiency conversion between the GT cycle and the bottoming ORC-based systems. This high exergy destruction results in low useful heat transfer rate to be transferred to the bottoming cycle. As a result of low transferred useful heat to the bottoming cycle, less power is produced. Henceforth, firstly, the present study solves this issue by employing a CLBC between the bottoming cycle and the topping cycle to decrease the thermal mismatch between the two systems. Second, as a result of this inclusion, the power conversion efficiency increases, and hence the present proposed system will be superior than those of the previously devised systems in terms of the power conversion factor. Thirdly, an LNG open power generation cycle is added to recover the exhaust gas temperature of the GT cycle via a preheater which also increases the overall power conversion efficiency while producing natural gas from its liquified form. The superiority of the developed system over the previously devised units is quantitatively expounded in the model comparison subsection of the study.

According to the literature review, waste heat recovery can comparatively increase the operational performance of a biogas-driven Bryton cycle. However, efficient waste management and modification of conventional designs are economically and environmentally essential. With this motivation, this study proposes a novel model of waste heat recovery for a GT cycle fueled by biogas, benefitting from a highly -efficient and advanced operational mode. This model consists of a CLBC, a dual-stage CCP unit composed of an ORC using R245fa as the working fluid integrated with an ERC, and a LNG-based power plant. The principal purposes of the current investigation can be summarized as follows:

The proposed waste heat recovery for the biogas-fed GT cycle increases the net output power in three different stages using a CLBC, an ORC, and a LNG open power generation cycle.

It is possible to yield cooling through an ERC as a boosting tool integrated with the ORC.

The cascade waste management proposed in the current study thermodynamically and economically increases the ability of operation compared to similar works.

A sensitivity analysis is carried out.

A comprehensive thermodynamic- and economic-based parametric study along with a multi-objective optimization using a genetic algorithm is done.

2- Description of system

The suggested biogas-driven cogeneration system for simultaneous supply of electricity and cooling is displayed in Fig. 1. The set-up consists of four sub-sets including a GT cycle fed by biogas, a CLBC, a two-stage CCP composed of an ORC combined with an ERC, and a LNG power generation system.

In explanation of the GT cycle, the air at ambient conditions flows into the compressor to be pressurized, then enters the combustion chamber for combusting the supplied

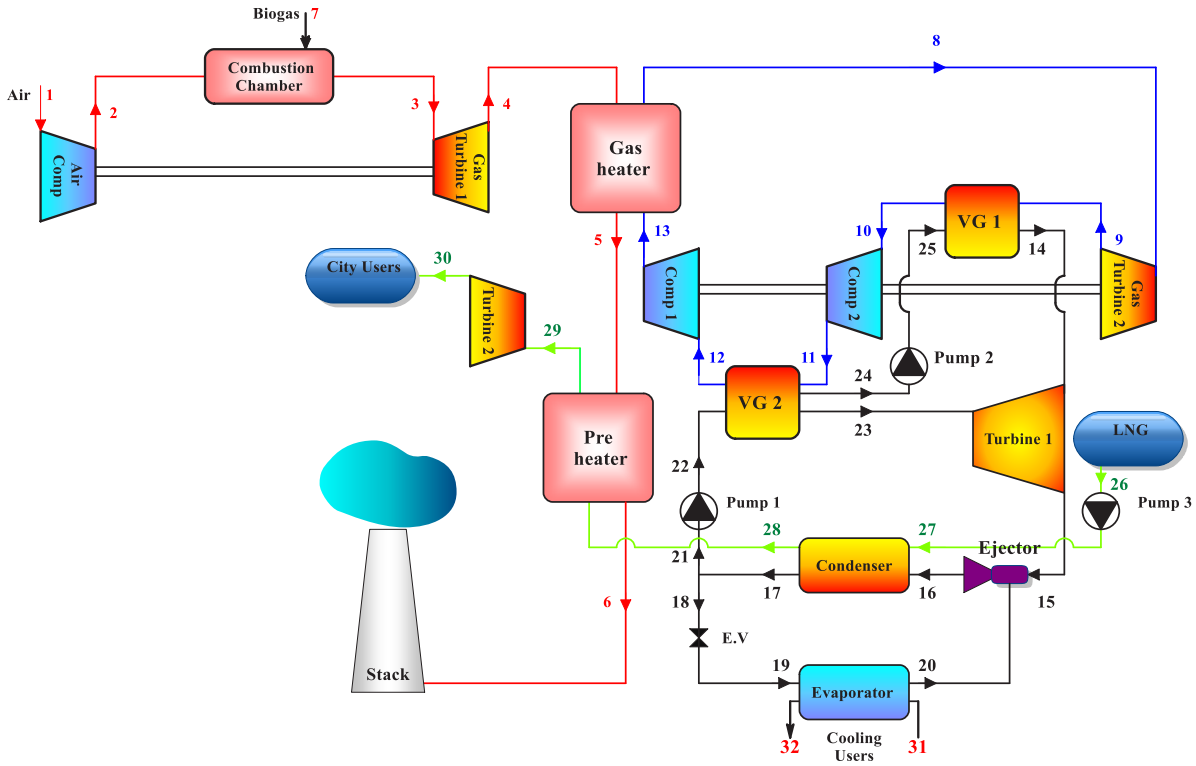

Fig. 1. Proposed CCP system fueled by biogas and LNG.

biogas. After this process, a high-level energetic stream is sent into the GT for power generation. After that, the hot flue to exhaust the GT cycle directly goes into the gas heater (GH) to run the CLBC, then is sent into the preheater (PH) to transfer its extra heating capacity to the natural gas (NG) stream.

In the CLBC, supercritical CO_2 is used as a working fluid inside the loop. In this process, supercritical CO_2 is expanded through gas turbine 2 and then transfers its heating capacity to the dual-stage CCP via vapor generator 1 (VG 1). Here, CO_2 is compressed and then cooled down as saturated vapor via VG2. Then, this stream is compressed into supercritical CO_2 via compressor 1.

In the two-stage CCP cycle, the heat-based energy of the CLBC is extracted through two stages. First, the saturated vapor is fed into the first turbine and then is used as the primely stream of the ejector. While the primary flow sucks the secondary one into the ejector, the mixed flow is ejected from the ejector toward the condenser. The flow is condensed through the condenser and is split into two streams. One is directed toward an expansion device to attain the evaporator pressure and then is directed to the ejector. The second flow is streamed toward the vapor generator 2 by using some mechanical power for pumping. The outlet stream of VG2 is split into two streams. One stream is fed into turbine 1, while the second stream is pumped back to the VG 2 pressure via pump 2, finishing the two-stage CCP process.

In the LNG open power generation unit, the LNG stored in a tank is pressurized to the required pressure level through an isentropic process and then its energy is recovered via two stages of condenser and precooler. Next, it is expended through the second turbine and is utilized as NG.

3- Thermal modeling and presumptions

3- 1- Thermodynamic presumptions

The following presumptions are regarded through thermal modeling of the devised cogeneration set-up:

The simulation and its report are achieved under steady state presumption.

For the expansion/compression processes occurring during the simulation, a constant isentropic efficiency is presumed.

Ideal gas assumption for the gas mixture is made [17, 18].

2% of fuel LHV is presumed as thermal loss of the combustion [19].

4% pressure drop is presumed for the combustion chamber [1].

The biogas is constituted of 60% of methane and 40% of CO_2 [15, 17].

The air is constituted 77.48% of N_2, 20.59% of O_2, 0.03% of Co_2, and 1.9% of H_2O the [19].

In addition, the required quantitative data and assumptions are listed in Table 1.

Table 1. Input parameters for similutaion [20-24].

Parameter	value
Dead state pressure, $P_0\,(\mathrm{kPa})$	101.3
Dead state temperature, $T_0\,(\mathrm{K})$	293.2
AC pressure ratio, r_{AC}	10
GT isentropic efficiency, $\eta_{GT}\,(\%)$	86
GT 1 inlet temperature, $T_3\,(\mathrm{K})$	1300
AC isentropic efficiency, $\eta_{AC}\,(\%)$	86
GT 2 inlet temperature, $T_8\,(\mathrm{K})$	720
Net power of GT cycle, $\dot{W}_{net,GT}\,(\mathrm{kW})$	1000
GT 2 outlet pressure, $P_9\,(\mathrm{kPa})$	3000
GT 2 inlet pressure, $P_8\,(\mathrm{kPa})$	40000
Turbine 1 outlet pressure, $P_{15}\,(\mathrm{kPa})$	420
Condenser pressure, $P_{cond}\,(\mathrm{kPa})$	120
Vapor generator 1 temperature, $T_{VG1}\,(\mathrm{K})$	415
Vapor generator 2 pressure, $P_{VG2}\,(\mathrm{kPa})$	1500
Evaporator temperature, $T_{Eva}\,(\mathrm{K})$	258
LNG turbine 2 inlet, $P_{28}\,(\mathrm{kPa})$	3000
Nozzle efficiency of ejector, η_{Noz}	0.85
Compressor isentropic efficiency, $\eta_{Comp}\,(\%)$	86
Turbine isentropic efficiency, $\eta_{tur}\,(\%)$	86
Diffuser efficiency of ejector, $\eta_{Dif}\,(\%)$	85
Pump isentropic efficiency, $\eta_{Pu}\,(\%)$	90
Mixer efficiency of ejector , $\eta_{Mix}\,(\%)$	90
TTD of vapor generator 1, $TTD_{VG1}\,(\mathrm{K})$	20
TTD of gas heater, $TTD_{GH}\,(\mathrm{K})$	20
TTD of preheater, $TTD_{PH}\,(\mathrm{K})$	10
TTD of vapor generator 2, $TTD_{VG2}\,(\mathrm{K})$	10
TTD of codenser, $TTD_{cond}\,(\mathrm{K})$	10
PPTD of evaporator, $\Delta T_{PP,Eva}\,(\mathrm{K})$	2
Evaporator inlet water temperature, $T_{W,Eva}\,(\mathrm{K})$	273

3- 2- Thermodynamic analysis

Using mass and energy conservative equations in general form, the mass and enthalpy required for a specific state can be computed as:

Mass balance relation:

$$\sum \dot{m}_{in,k} - \sum \dot{m}_{out,k} = 0 \tag{1}$$

where $\dot{m}$ is the mass flow rate.

Energy balance relation:

$$\dot{Q}_k - \dot{W}_k = \sum \dot{m}_{out,k}\left(h_{out,k}\right) - \sum \dot{m}_{in,k}\left(h_{in,k}\right) \tag{2}$$

where $\dot{Q}_k$ is the heat transfer rate, $\dot{W}_k$ is the power, and h is the specific enthalpy.

The mathematical modeling of the GT cycle is explained comprehensively in our previous study and are excluded here [14, 16].

The balance equation based on the second law analysis for the kth constituent of a set-up is articulated as [25]:

$$\dot{E}x_{D,k} = \sum_i \dot{E}x_{in,k} - \sum_e \dot{E}x_{out,k} \tag{3}$$

where $\dot{E}x_{D,k}$ is its exergy destruction rate, and $\dot{E}x_{in,k}$ and $\dot{E}x_{out,k}$ are the exergy flow rates entering and exiting the kth constituent, respectively.

Accounting only physical and chemical exergy values in the mathematical modeling of the simulated unit, we then have [25]:

$$\dot{E}x_k = \dot{E}x_{ph,k} + \dot{E}x_{ch,k} \tag{4}$$

where $\dot{E}x_{ph,k}$ and $\dot{E}x_{ch,k}$ are physical and chemical exergy rates of the kth constituent formulated as:

$$\dot{E}x_{\mathrm{ph,k}} = \dot{m}(h - h_0 - T_0(s - s_0))_k \tag{5}$$

$$\dot{E}x_{\mathrm{ch,k}} = \dot{m}(\sum_i y_i \overline{ex}_i^{ch,0} + \bar{R}T_0 \sum_i y_i \ln y_i)_k \tag{6}$$

Here, s is the specific entropy, $\bar{R}$ is the universal gas constant, y_i the molar fraction of ith compound, and $\overline{ex}_i^{ch,0}$ is its standard chemical exergy [26].

The exergetic efficiency of a system is defined as [26]:

$$\eta_{ex,k} = \frac{\dot{E}x_{out}}{\dot{E}x_{in}} = \frac{\dot{E}x_{prod,k}}{\dot{E}x_{fuel,k}} \tag{7}$$

The employed energy and exergy relations for the simulated unit are listed in Table 2.

3- 3- Economic analysis

Accounting cost of operating, capital investment ($\dot{Z}_{total}^{CL}$), maintenance of equipment ($\dot{Z}_{total}^{OM}$), cost associated with heat transfer ($\dot{C}_{Q,k}$) and electricity ($\dot{C}_{W,k}$) consumed during the process, and any extra entering ($\dot{C}_{in,k}$) or exiting ($\dot{C}_{out,k}$) streams from an element, the cost balance equation can be articulated in terms of the appointed metrics as follows [25]:

$$\dot{C}_{Q,k} = \sum \dot{C}_{in,k} + \dot{Z}_{total}^{OM} + \dot{Z}_{total}^{CL} = \dot{C}_{W,k} + \sum \dot{C}_{out,k} \tag{8}$$

Genarlly,

$$\dot{C}_k = c_k \dot{E}x_k \tag{9}$$

Here, c is the cost per unit exergy in $\$/\mathrm{GJ}$.

The cost rate of exergy destruction for the kth element ($\dot{C}_{D,k}$) is expressed as [29]:

$$\dot{C}_{D,k} = c_{P,k} \dot{E}x_{D,k} \tag{10}$$

In Eq. (8), the sum of cost rate associated with operating, maintenance, and capital investment can be expressed in a unit parameter as [29]:

$$\dot{Z}_k = \dot{Z}_{total}^{OM} + \dot{Z}_{total}^{CL} = CRF \times \frac{\varphi_r \times 365 \times 24}{\mathrm{N}} \times Z_k \tag{11}$$

in which $N = 8000$ is the annual operating number of the plant, $\dot{Z}_k$ is the purchase cost function, $i_r = 0.05$ is the interest rate, $\varphi_r = 0.15$ is the maintenance factor, and $n_r = 20yr$ is the life time of the system [30]. CRF stands for the capital recovery factor and is expressed as [29]:

$$CRF = \frac{i_r\left(1+i_r\right)^{n_r}}{\left(1+i_r\right)^{n_r} - 1} \tag{12}$$

Similar to the exergy balance equation which is stated in terms of product, fuel, loss, and destruction, the same cost

Table 2. Mass, energy, and exergy balance equations utilized for components.

Components	Energy balance equations	Exergy balance equations
GT cycle [14]		
Air compressor	$\dot{W}_{AC}=\dot{m}_1(h_2-h_1)$, $\eta_{is,AC}=h_1-h_{2s}/h_1-h_2$	$\dot{W}_{AC}-(\dot{E}x_2-\dot{E}x_1)$
Combustion chamber	$-0.02\lambda LHV+h_a+\lambda h_f-(1+\lambda)h_p=LHV\times\dot{m}_f/\dot{M}_f$ $\dot{Q}_{CC}=\dot{m}_{fuel}LHV$	$(\dot{E}x_2+\dot{E}x_7)-\dot{E}x_3$
Gas turbine 1	$\dot{W}_{GT1}=\dot{m}_4(h_4-h_5)$, $\eta_{is,GT}=(h_4-h_5)/(h_4-h_{5s})$	$(\dot{E}x_4-\dot{E}x_5)-\dot{W}_{GT1}$
CLBC [27, 28]		
Gas heater	$\dot{Q}_{GH}=\dot{m}_4(h_4-h_5)$, $\dot{Q}_{GH}=\dot{m}_8(h_8-h_{13})$	$(\dot{E}x_4-\dot{E}x_5)-(\dot{E}x_8-\dot{E}x_{13})$
Gas turbine 2	$\dot{W}_{GT2}=\dot{m}_8(h_8-h_9)$, $\eta_{is,GT}=(h_8-h_9)/(h_8-h_{9s})$	$(\dot{E}x_8-\dot{E}x_9)-\dot{W}_{GT2}$
Compressor 1	$\dot{W}_{comp1}=\dot{m}_{12}(h_{13}-h_{12})$, $\eta_{is,comp}=h_{12}-h_{13s}/h_{12}-h_{13}$	$\dot{W}_{comp1}-(\dot{E}x_{13}-\dot{E}x_{12})$
Compressor 2	$\dot{W}_{comp2}=\dot{m}_{11}(h_{11}-h_{10})$, $\eta_{is,comp}=h_{10}-h_{11s}/h_{10}-h_{11}$	$\dot{W}_{comp2}-(\dot{E}x_{11}-\dot{E}x_{10})$
Two-stage CCP system [15]		
Vapor generator 1	$\dot{Q}_{VG1}=\dot{m}_{10}(h_9-h_{10})$, $\dot{Q}_{VG1}=\dot{m}_9(h_{14}-h_{25})$	$(\dot{E}x_9-\dot{E}x_{10})-(\dot{E}x_{14}-\dot{E}x_{25})$
Vapor generator 2	$\dot{Q}_{VG2}=\dot{m}_{10}(h_{10}-h_{11})$, $\dot{Q}_{VG2}=\dot{m}_{24}(h_{24}-h_{22})+\dot{m}_{23}(h_{23}-h_{22})$	$(\dot{E}x_{11}-\dot{E}x_{12})-(\dot{E}x_{23}+\dot{E}x_{24}-\dot{E}x_{22})$
Turbine 1	$\dot{W}_{tur1}=\dot{m}_{15}(h_{14}-h_{15})+\dot{m}_{23}(h_{23}-h_{15})$, $\eta_{is,tur}=(h_{14}-h_{15})/(h_{14}-h_{15s})$	$(\dot{E}x_{23}+\dot{E}x_{14}-\dot{E}x_{15})-\dot{W}_{tur1}$
Ejector	-	$(\dot{E}x_{20}+\dot{E}x_{15})-\dot{E}x_{16}$
Evaporator	$\dot{Q}_{eva}=\dot{m}_{19}(h_{20}-h_{19})$, $\dot{Q}_{eva}=\dot{m}_{31}(h_{32}-h_{31})$	$(\dot{E}x_{20}-\dot{E}x_{19})-(\dot{E}x_{32}-\dot{E}x_{31})$
Condenser	$\dot{Q}_{cond}=\dot{m}_{16}(h_{28}-h_{27})$, $\dot{Q}_{cond}=\dot{m}_{16}(h_{16}-h_{17})$	$(\dot{E}x_{27}-\dot{E}x_{28})-(\dot{E}x_{16}-\dot{E}x_{17})$
Pump 1	$\dot{W}_{Pu1}=\dot{m}_{20}(h_{22}-h_{21})$, $\eta_{is,Pu}=(h_{22s}-h_{21})/(h_{22}-h_{21})$	$\dot{W}_{Pu1}-(\dot{E}x_{22}-\dot{E}x_{21})$
Pump 2	$\dot{W}_{Pu2}=\dot{m}_{24}(h_{25}-h_{24})$, $\eta_{is,Pu}=(h_{25s}-h_{23})/(h_{25}-h_{23})$	$\dot{W}_{Pu2}-(\dot{E}x_{25}-\dot{E}x_{24})$
LNG power generation system [29]		
Pump 3	$\dot{W}_{Pu3}=\dot{m}_{26}(h_{27}-h_{26})$, $\eta_{is,Pu}=(h_{27s}-h_{26})/(h_{27}-h_{26})$	$\dot{W}_{Pu3}-(\dot{E}x_{27}-\dot{E}x_{26})$
Turbine 2	$\dot{W}_{tur2}=\dot{m}_{29}(h_{29}-h_{30})$, $\eta_{is,tur}=(h_{29}-h_{30})/(h_{29}-h_{30s})$	$(\dot{E}x_{29}-\dot{E}x_{30})-\dot{W}_{tur2}$
Preheater	$\dot{Q}_{PH}=\dot{m}_{28}(h_{29}-h_{27})$, $\dot{Q}_{PH}=\dot{m}_6(h_5-h_6)$	$(\dot{E}x_5-\dot{E}x_{196})-(\dot{E}x_{29}-\dot{E}x_{28})$

Table 3. The overall heat transfer coefficient of heat exchangers.

Component	U_k (W/m²K)	Reference
Air preheater	500	[14]
Vapor generator	30	[14]
Evaporator	1000	[14]

balance equation in terms of the appointed metrics can be expressed as follows [29]:

$$\dot{C}_{P,total} = \dot{C}_{F,total} + \dot{Z}^{OM}_{total} + \dot{Z}^{CL}_{total} \quad (13)$$

The fuel price is assumed 7.36 $/GJ [30].

The exergoeconomic factor (f_k) and relative cost difference (r_k) are defined respectively as [29]:

$$f_k = \frac{\dot{Z}_k}{\dot{Z}_k + \dot{Z}_{D,k}} \quad (14)$$

$$r_k = \frac{c_{Pr,k} - c_{F,k}}{c_{F,k}} \quad (15)$$

The total heat transfer area can be computed as [29]:

$$A_k = \frac{\dot{Q}_k}{U_k \times \Delta T_{LMTD}} \quad (16)$$

where ΔT_{LMTD} is the logarithmic mean temperature difference and U_k is the total heat transfer coefficient for heat transfer-based elements tabulated in Table 3.

The economic equations needed for economic analysis of the simulated system are given in Table 4.

3- 4- Major performance criteria

The energetic efficiency of the GT cycle is given as [15]:

$$\eta_{en,GT} = \frac{\dot{W}_{GT1} - \dot{W}_{AC}}{\dot{n}_{Biogas}\overline{LHV}_{Biogas}} \quad (17)$$

where $\overline{LHV}_{Biogas}$ refers to the lower heating value of the biogas.

The energetic efficiency of the combined GT-CLBC unit is defined [15]:

$$\eta_{en,GT-CLBC} = \frac{\dot{W}_{net,GT-CLBC}}{\dot{n}_{Biogas}\overline{LHV}_{Biogas}} \quad (18)$$

Where

$$\dot{W}_{net,GT-CLBC} = \dot{W}_{GT1} + \dot{W}_{GT2} - \dot{W}_{AC} - \dot{W}_{Comp1} - \dot{W}_{Comp2} \quad (19)$$

The energetic efficiency of the overall integrated cogeneration system may be stated as follows [15]:

$$\eta_{en,cog} = \frac{\dot{W}_{net,cog} - \dot{Q}_{Eva}}{\dot{n}_{Biogas}\overline{LHV}_{Biogas}} \quad (20)$$

Where

$$\dot{W}_{net,cog} = \dot{W}_{GT1} + \dot{W}_{GT2} - \dot{W}_{AC} - \dot{W}_{Comp1} - \dot{W}_{Comp2} + \dot{W}_{tur1} + \dot{W}_{tur2} - \dot{W}_{Pu1} - \dot{W}_{Pu2} - \dot{W}_{Pu3} \quad (21)$$

The exergetic efficiency of the GT cycle is defined as [15]:

$$\eta_{ex,GT} = \frac{\dot{W}_{GT1} - \dot{W}_{AC}}{\dot{n}_{Biogas}\overline{\overline{ex}}^{0}_{ch,Biogas}} \quad (22)$$

The exergetic efficiency of the combined GT-CLBC unit is articulated as [15]:

$$\eta_{ex,GT-CLBC} = \frac{\dot{W}_{net,GT-CLBC}}{\dot{n}_{Biogas}\overline{\overline{ex}}^{0}_{ch,Biogas}} \quad (23)$$

Table 4. Cost-based equations utilized for components.

Components	Cost balance equations	Auxiliary equations	Equipment cost function*
GT cycle [14]			
Air compressor	$\dot{C}_2 = \dot{C}_1 + \dot{Z}_{AC} + \dot{C}_{w,AC}$	$c_{W,AC} = c_{W,GT1}$ $c_1 = 0$	$Z_{AC} = (71.1\dot{m}_1 / (0.9 - \eta_{is,AC}))(P_2 / P_1)\ln(P_2 / P_1)$
Combustion chamber	$\dot{C}_3 = \dot{C}_2 + \dot{C}_{Fuel} + \dot{Z}_{CC}$	$\dot{C}_{Fuel} = FP \times \dot{n}_{Fuel} \times LHV$	$Z_{CC} = (46.08\dot{m}_3 / (0.995 - P_4 / P_3))$ $[1 + \exp(0.018T_4 - 26.4)]$
Gas turbine1	$\dot{C}_4 + \dot{C}_{w,GT1} = \dot{C}_3 + \dot{Z}_{GT1}$	$c_4 = c_3$	$Z_{GT1} = (479.34\dot{m}_3 / (0.92 - \eta_{is,GT}))$ $\ln(P_3 / P_4)[1 + \exp(0.036T_3 - 54.4)]$
CLBC [15]			
Gas heater	$\dot{C}_4 + \dot{C}_{13} + \dot{Z}_{GH} = \dot{C}_5 + \dot{C}_6$	$c_4 = c_5$	$Z_{GH} = 130 \times \left(A_{GH} / 0.093\right)^{0.78}$
Gas turbine2	$\dot{C}_9 + \dot{C}_{w,GT2} = \dot{C}_8 + \dot{Z}_{GT2}$	$c_8 = c_9$	$Z_{GT2} = (479.34\dot{m}_8 / (0.92 - \eta_{is,GT}))$ $\ln(P_8 / P_9)[1 + \exp(0.036T_8 - 54.4)]$
Compressor 1	$\dot{C}_{13} = \dot{C}_{12} + \dot{Z}_{comp1} + \dot{C}_{w,comp1}$	$c_{W,comp1} = c_{W,GT2}$	$Z_{comp1} = (71.1\dot{m}_{12} / (0.9 - \eta_{is,comp}))(P_{13} / P_{12})$ $\ln(P_{13} / P_{12})$
Compressor 2	$\dot{C}_{11} = \dot{C}_{10} + \dot{Z}_{comp2} + \dot{C}_{w,comp2}$	$c_{W,comp2} = c_{W,GT2}$	$Z_{comp1} = (71.1\dot{m}_{10} / (0.9 - \eta_{is,comp}))(P_{10} / P_{11})$ $\ln(P_{10} / P_{11})$
Two-stage CCP system [15]			
Vapor generator 1	$\dot{C}_9 + \dot{C}_{25} + \dot{Z}_{VG1} = \dot{C}_{10} + \dot{C}_{14}$	$c_9 = c_{10}$	$Z_{VG1} = 130 \times \left(A_{VG1} / 0.093\right)^{0.78}$
Vapor generator 2	$\dot{C}_{11} + \dot{C}_{22} + \dot{Z}_{VG2} = \dot{C}_{12} + \dot{C}_{23} + \dot{C}_{24}$	$c_{11} = c_{12}$	$Z_{VG2} = 130 \times \left(A_{VG2} / 0.093\right)^{0.78}$
Turbine 1	$\dot{C}_{15} + \dot{C}_{w,tur1} = \dot{C}_{23} + \dot{Z}_{tur1} + \dot{C}_{14}$	$c_{14} = c_{15}$	$Z_{tur1} = (1536\dot{m}_{14} / (0.93 - \eta_{is,tur}))$ $\ln(P_{14} / P_{15})[1 + \exp(0.036T_{14} - 54.4)]$
Ejector	$\dot{C}_{15} + \dot{C}_{20} = \dot{Z}_{ej} + \dot{C}_{16}$	-	$\dot{Z}_{ej} = 0$
Condenser	$\dot{C}_{16} + \dot{C}_{27} + \dot{Z}_{cond} = \dot{C}_{17} + \dot{C}_{28}$	$c_{16} = c_{17}$	$Z_{cond} = 130 \times \left(A_{cond} / 0.093\right)^{0.78}$
Evaporator	$\dot{C}_{31} + \dot{C}_{19} + \dot{Z}_{eva} = \dot{C}_{32} + \dot{C}_{20}$	$c_{19} = c_{20}$	$Z_{eva} = 130 \times \left(A_{eva} / 0.093\right)^{0.78}$
Pump 1	$\dot{C}_{22} = \dot{C}_{21} + \dot{Z}_{Pu1} + \dot{C}_{W,Pu1}$	$c_{W,Pu1} = c_{W,tur1}$	$Z_{Pu1} = 3540 \times \left(\dot{W}_{Pu1}\right)^{0.71}$
Pump 2	$\dot{C}_{25} = \dot{C}_{24} + \dot{Z}_{Pu2} + \dot{C}_{W,Pu2}$	$c_{W,Pu2} = c_{W,tur2}$	$Z_{Pu2} = 3540 \times \left(\dot{W}_{Pu2}\right)^{0.71}$
LNG power generation system [29]			
Pump 3	$\dot{C}_{27} = \dot{C}_{26} + \dot{Z}_{Pu3} + \dot{C}_{W,Pu3}$	$c_{W,Pu3} = c_{W,tur2}$	$Z_{Pu3} = 3540 \times \left(\dot{W}_{Pu3}\right)^{0.71}$
Turbine 2	$\dot{C}_{29} + \dot{C}_{w,tur2} = \dot{C}_{30} + \dot{Z}_{tur2}$	$c_{30} = c_{29}$	$Z_{tur2} = (1536\dot{m}_{29} / (0.93 - \eta_{is,tur}))$ $\ln(P_{29} / P_{30})[1 + \exp(0.036T_{29} - 54.4)]$
Preheater	$\dot{C}_5 + \dot{C}_{28} + \dot{Z}_{PH} = \dot{C}_6 + \dot{C}_{29}$	$c_5 = c_6$	$Z_{PH} = 130 \times \left(A_{PH} / 0.093\right)^{0.78}$
Division point	$\dot{C}_{17} = \dot{C}_{18} + \dot{C}_{21}$	$c_{17} = c_{18} = c_{21}$	-

*Ref. [18] **Ref. [30]

Table 5. Settings for the genetic algorithm [16, 31].

Settings	Value
Number of generations	64
Individuals number in the population	32
Initial mutation rate	0.25
Maximum mutation rate	0.25
Crossover probability	0.85
Minimum mutation rate	0.0005

The exergetic efficiency of the overall integrated cogeneration unit is defined as [15]:

$$\eta_{ex,cog}=\frac{\dot{W}_{net,cog}+(\dot{E}x_{32}-\dot{E}x_{31})}{\dot{n}_{Biogas}\overline{\overline{ex}}^{0}_{ch,Biogas}+(\dot{E}x_{30}-\dot{E}x_{26})} \quad (24)$$

The unit overall product cost (UOPC) for the GT cycle may be stated as follows [15]:

$$UOPC_{GT}=\frac{\dot{C}_{W,GT1}-\dot{C}_{W,AC}}{\dot{C}_{GT1}-\dot{W}_{AC}} \quad (25)$$

The UOPC for the combined GT-CLBC system may be stated as follows [15]:

$$UOPC_{GT-CLBC}=\frac{\dot{C}_{W,GT-CLBC}}{\dot{C}_{net,GT-CLBC}} \quad (26)$$

Where

$$\begin{aligned}\dot{C}_{W,GT-CLBC}&=\dot{C}_{W,GT1}+\dot{C}_{W,GT2}\\&-\dot{C}_{W,AC}-\dot{C}_{W,Comp1}-\dot{C}_{W,Comp2}\end{aligned} \quad (27)$$

The UOPC for the overall integrated cogeneration system may be stated as follows :

$$UOPC_{GT-cog}=\frac{\dot{C}_{W,cog}+\dot{C}_{32}}{\dot{W}_{net,cog}+\dot{E}x_{32}} \quad (28)$$

Where $\dot{C}_{32}$ is the cost rate of the released cold exergy of the evaporator and $\dot{C}_{W,cog}$ is the cost rate of the net electricity of cogeneration system.

$$\begin{aligned}\dot{C}_{W,CLBC}&=\dot{C}_{W,GT1}+\dot{C}_{W,GT2}+\dot{C}_{W,tur1}+\dot{C}_{W,tur2}\\&-\dot{C}_{W,AC}-\dot{C}_{W,Comp1}-\dot{C}_{W,Comp2}-\dot{C}_{W,Pu1}-\dot{C}_{W,Pu2}-\dot{C}_{W,Pu3}\end{aligned} \quad (29)$$

4- Multi-criteria optimization

The optimization allows for finding out the best operating condition and enhancing the system's ability, especially when the multigeneration framework is devised. On this account, this study suggests and performs multi-objective optimization strategies of the studied system in the present work. Despite this fact, a genetic algorithm is adopted and implemented in this work benefiting from a smart search phenome in an evolutionary algorithm leading to determining the best solution. The genetic algorithm has been considered in some previous studies and has exhibited good interaction with energy systems [15]. Thus, this study utilizes the algorithm thanks to three objective functions (η_{en} , η_{ex} , and $UOPC_{sys}$). Table 5 exhibits the settings for this algorithm in the EES software. Subsequently, these functions are optimized solely at first, then the multi-objective function (*MOO*) written in Eq. (31) is provided for the multi-objective optimization. Indeed, this function embraces a weight coefficient (w) of $1/3$ for each objective function16]].

Three design parameters of the energy and exergy efficiencies and UOPC are reckoned as objective functions. The selected decision variables are:

$$\begin{aligned}&8\le r_{AC}\le 15;\\&115\le P_{cond}(\text{kPa})\le 124;\\&20000\le P_8(\text{kPa})\le 60000;\\&2000\le P_9(\text{kPa})\le 5000;\\&320\le P_{15}(\text{kPa})\le 820;\\&500\le P_{23}(\text{kPa})\le 1800;\\&1200\le T_3(\text{K})\le 1550;\\&250\le T_{eva}(\text{K})\le 265;\\&680\le T_8(\text{K})\le 780;\\&410\le T_{14}(\text{K})\le 420;\end{aligned} \quad (30)$$

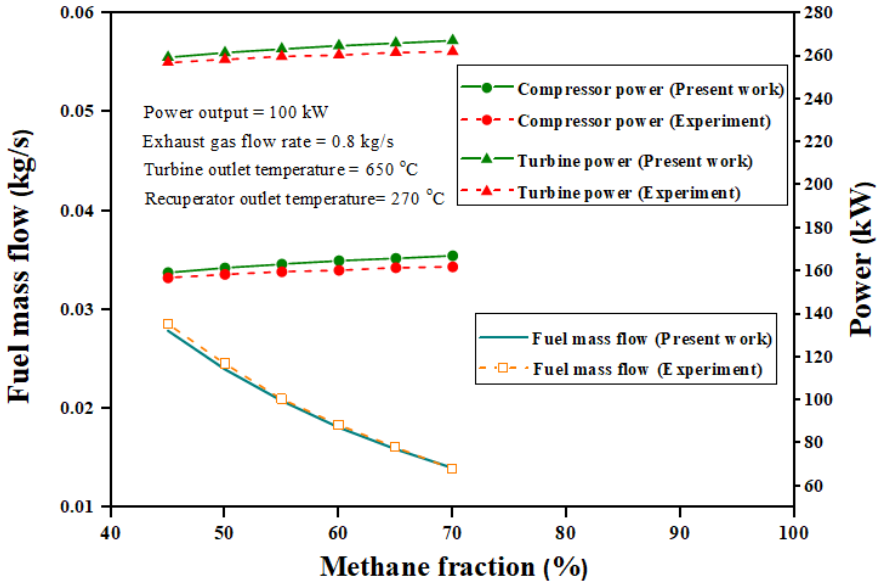

Fig. 2. Validation of the Brayton cycle with Somehsaraei et al. [32] study.

The simultaneous target of maximizing thermal and exergy efficiencies and minimizing UOPC is achieved by defining a multi-objective operator (MOO) as follows [16]:

$$Max\,(MOO = w_1 \times \eta_{en} + w_2 \times \eta_{ex} + w_3 \times (1 - \frac{UOPC_{sys}}{c_7}) \quad (31)$$

$$w_1 + w_2 + w_3 = 1; 0 \le w_1, w_2, w_3 \le 1 \quad (32)$$

Here, w is the weight coefficient for each objective. Also, c_7 is the biogas unit cost.

5- Results and discussion

5- 1- Model verification

The validity of the model developed for the main components and subsystems is verified in this subchapter. Fig. 2 reveals the validation of the Brayton cycle and Table 6 prove the precision of the ejector model.

According to Fig. 2, the result of the study by Somehsaraei et al. [32] is used to validate the result of the biogas-fed Brayton cycle in the present work. In this regard, the power consumed by the air compressor, the power produced by the gas turbine, and the mass flow rate of the inlet fuel against the variation in the methane fraction are obtained and compared. Here, the margin of error is below 3%.

Using different pressures and temperatures for the input terminals of the ejector and different condenser's operating temperatures based on numerical and experimental studies by Huang et al. [33], the entrainment ratio of the ejector is computed and compared with Ref. [33] (see Table 6). The absolute error between this study and numerical and experimental models in Ref. [25] are 4.7% and 4.1%, respectively.

5- 2- Model comparison

In this section, the main pros and cons of the current developed biogas-driven cogeneration system is discussed by comparing its chief performance metrics with a similar study in the literature, i.e., Ref. [15]. In this study, we aim at improving performance of the previous developed biogas-driven cogeneration system in terms of extracting more electricity by proposing an efficient waste management. The main difference between the present cogeneration system and those reported in Ref. [15] in terms of layout is using a CLBC between the GT cycle and the ORC-based unit for extracting more electricity via an appropriate set-up. Another difference is inclusion of the LNG power generation set-up for recovering exhaust gases energy released from the gas heater of the CLBC for regasification purposes. There are also some minor differences in the layouts of both systems, including the employment of two-stage ORC in the combined ORC-ERC system for capturing more energy from the CLBC which also improves overall performance of the unit. The previous developed model was applicable for two cooling temperature levels which are not accounted here, although it can be extended based on the given data in previous model.

In order to have a real comparison, it is imperative to set a same input condition for both systems. For this aim, air compressor ratio is fixed at 10, gas turbine inlet temperature

Table 6. Validation of ejector simulation with Huang et al. [33] study.

P_{pf} (Mpa); T_{pf} (°C)	P_{sf} (Mpa); T_{sf} (°C)	T_{cond} (°C)	$\mu = \dot{m}_{sf} / \dot{m}_{pf}$			Error$_1$ (%)	Erorr$_2$ (%)
			This work	Numerical model [30]	Experimental [30]		
0.604;95	0.04;8	42.1	0.1621	0.1554	0.1859	4.31	12.8
0.538;90	0.04;8	38.9	0.2201	0.2156	0.2246	2.08	2
0.465;84	0.04;8	35.5	0.2804	0.2880	0.2880	2.63	2.63
0.4;78	0.04;8	32.5	0.3334	0.3525	0.3257	5.41	2.36
0.604;95	0.0473;12	42.5	0.2402	0.2573	0.2350	6.64	2.21
0.538;90	0.0473;12	39.5	0.3023	0.3257	0.2946	7.18	2.91

Table 7. Comparison results between the current developed cogeneration system and thoes reported in Ref. [15].

Parameters	Present study	Ref. [15]
Net power, (kW)	1927	1189
Cooling load, (kW)	241.7	320.5
Total exergy destruction, (kW)	2891	2046
Energy efficiency, (%)	66.98	49.07
Exergy efficiency, (%)	38.86	37.37
Overall product cost, ($/GJ)	10.89	14.44

is given 1300 K, the evaporators temperature is set on 258 K, and net power of the GT cycle is fixed at 1000 kW to investigate the effects of the bottoming cycles included in both studies. The ambient temperature and pressure are assumed at 293.2 K and 101.3 kPa, respectively. The results indicate that net power production value is surged from 1189 kW to 1927 kW, indicating over 62% improvement. However, the cooling production is decreased by 24.58%, which is mainly reflects the fact that previous model has two evaporators which leads to more cooling production. Another disadvantage of the present model is its high exergy destruction rate which is mainly due to employment of the CLBC. However, the energy and exergy efficiencies are improved by 36.5% and 4%, respectively, indicating that the first and second laws analysis substantiate the present model versus the previous cogeneration system. In terms of thermoeconomic, overall product cost of the previous model is around 23% higher than the present study, and hence present model is economically more feasible.

5- 3- Sensitivity analysis

In order to find out the most influential parameter affecting the system's operation from the thermodynamic and economic points of view, the relevant sensitivity index is measured and indicated in Fig. 3. The sensitivity index is a variable demonstrating the effect of variation in each decision parameter on the objective functions. Regarding the variation range of a decision variable, the sensitivity index is calculable by dividing the difference between the maximum and minimum values of an objective function into the sum of changes attained from all decision variables. Therefore, the sum of the sensitivity index for an objective function is equal to one. In this regard, referring to Fig. 3, the highest sensitivity index of the energy efficiency belongs to evaporator temperature (T_{eva}) at 0.246. GT 1 inlet temperature has second place with a value of 0.243. From the exergy efficiency point of view, the highest sensitivity index equals 0.534 respecting GT 1 inlet temperature (T_3), and the second-highest sensitivity index equals 0.116 respecting GT 2 inlet pressure (P_8). In addition, from the economic aspect, the highest sensitivity index of the UOPC belongs to GT 2 outlet pressure (P_9) with a value of 0.223. Then, GT 1 inlet temperature (T_3) has the second-highest sensitivity index at 0.173. Generally, GT 1 inlet temperature is introduced as the most influential parameter because it has the highest sensitivity index of energy efficiency and the second-highest sensitivity index of exergy efficiency and UOPC.

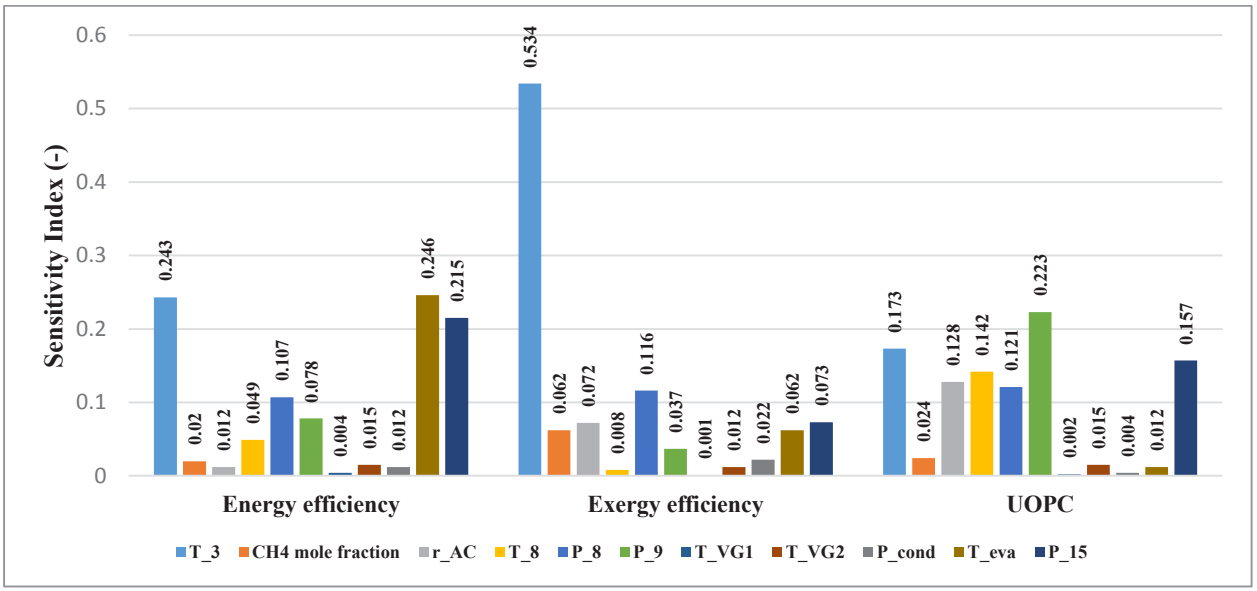

Fig. 3. Sensitivity index of decision variables on objective functions.

5- 4- Results of simulation

The results of optimization for the designed system are displayed in Fig. 4, presuming an equal weight coefficients ($w_1 = w_2 = w_3 = 1/3$) for each individual objective function. A comparative study of optimization between the base mode and optimum mode displays that both energy and exergy efficiencies are enhanced by 20.1% and 6.15%, individually. Also, the system's UOPC decreases by 7.52%, hence the attained optimum mode is preferable. Also, the conducted optimization exhibits that the introduced set-up augments the cooling capacity by 75.68%, whilst the net electricity reduces by 3.21%. Although the current optimization slightly reduces the generated power, it is recommended in order to increase the cooling load. To wrap it up, the optimum cooling load, net electricity, energy and exergy efficiencies, and UOPC of the CCP system are calculated at 424.1 kW, 1,864 kW, 80.4%, 41.24%, 10.07 $/GJ, respectively. At the optimum condition, decision variables are as follows: $r_{AC} = 14.57$, $T_3 = 1534(\mathrm{K})$, $T_{eva} = 265(\mathrm{K})$, $T_8 = 771.5(\mathrm{K})$, $P_8 = 36684(\mathrm{kPa})$, $P_9 = 4769(\mathrm{kPa})$, $T_{VG1} = 415(\mathrm{K})$, $P_{cond} = 116.5(\mathrm{kPa})$, $P_{VG2} = 1620(\mathrm{kPa})$, $P_{15} = 818.1(\mathrm{kPa})$.

Integration of the CLBC system with GT cycle leads to an improvement of the energy and exergy efficiencies by 32.93% and 32.92% in the base mode and 33.66% and 33.68% in the optimum mode, respectively. From the economic standpoint, the UOPC of the CLBC system compared to the GT cycle augments by 13.51% in the base mode, whilst it diminishes by 9.42% in the optimum mode.

Analogizing integration of the whole new CCP system with GT-CLBC cycle, the energy efficiency is improved by 63.06%, while the exergy efficiency declines so subtly in the base mode. However, in the optimum mode, the energy efficiency is improved by 71.17%, and exergy efficiency declines by 7.38%. From the economic aspect, the UOPC of the integrated CCP system compared to the GT-CLBC cycle declines by 19.45% in the base mode and 20.45% in the optimum mode.

Table 8 presents the role of each element in the overall exergetic and economic evaluation of the developed layout. The results proved that the high value of the overall exergy destruction stems from the combustion chamber by exergy destruction of 1,058 kW (for the base mode) and 775.2 kW (for the optimum mode) since these elements transfer high heat rate between the cold and hot streams. Among all components, gas turbines and gas heaters own the largest investment cost. The total cost rate related to the exergy destruction at the base and optimum modes were attained 70.16 $/h and 53.03 $/h, respectively. For a better understanding, the share of each element in exergy destruction is shown in Fig. 5.

5- 5- Parametric study

The effect of some chief thermodynamic parameters (i.e., gas turbine 1 inlet temperature, methane molar fraction, condenser pressure, gas turbine 2 inlet temperature, air compressor pressure ratio, gas turbine 2 inlet pressure, gas turbine 2 outlet pressure, vapor generator 1 temperature, vapor generator 2 pressure, evaporator temperature, and turbine 1 outlet pressure) on the major thermal and economic metrics is scrutinized in this part.

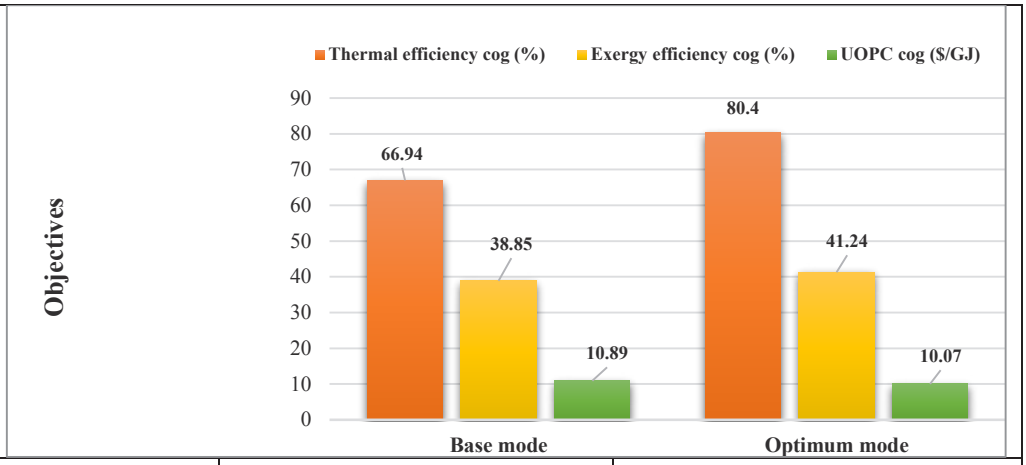

w_1	-	1/3
w_2	-	1/3
w_3	-	1/3
r_{AC}	10	14.57
T_3(K)	1300	1534
T_{eva}(K)	258	265
T_8(K)	720	771.5
P_8(kPa)	40000	36684
P_9(kPa)	3000	4769
T_{VG1}(K)	415	415
P_{cond}(kPa)	120	116.5
P_{VG1}(kPa)	1500	1620
P_{15}(kPa)	420	818.1
$\dot{Q}_{CC}$(kW)	3238	2846
$\dot{W}_{VG1}$(kW)	2130	1931
$\dot{W}_{VG2}$(kW)	908.9	637.1
$\dot{W}_{tur1}$(kW)	129.3	77.56
$\dot{W}_{tur2}$(kW)	490.9	474.9
$\dot{W}_{AC}$(kW)	1130	930.9
$\dot{W}_{comp1}$(kW)	269.1	199.2
$\dot{W}_{comp2}$(kW)	310.5	101.1
$\dot{W}_{net,cog}$(kW)	1926	1864
$\dot{Q}_{eva}$(kW)	241.4	424.1
μ	0.2574	0.5251

Fig. 4. Base case and optimum results of the proposed model.(Continued)

λ	0.05529	0.07279
$\eta_{en,GT}(\%)$	30.88	35.14
$\eta_{en,GT-CLPC}(\%)$	41.05	46.97
$\eta_{ex,GT}(\%)$	29.28	33.31
$\eta_{ex,GT-CLPC}(\%)$	38.92	44.53
$UOPC_{GT}(\$/GJ)$	11.91	11.57
$UOPC_{GT-CLBC}(\$/GJ)$	13.52	12.66

Fig. 4. Base case and optimum results of the proposed model.

Table 8. Comparison results between the current developed cogeneration system and thoes reported in Ref. [15].

Components	Base mode							Optimum mode						
	$\dot{E}x_{D,k}$ (kW)	$\dot{C}_{D,k}$ ($/h)	$\dot{Z}_k$ ($/h)	f_k (%)	r_k (%)	$\eta_{ex,k}$ (%)	y_D (%)	$\dot{E}x_{D,k}$ (kW)	$\dot{C}_{D,k}$ ($/h)	$\dot{Z}_k$ ($/h)	f_k (%)	r_k (%)	$\eta_{ex,k}$ (%)	y_D (%)
Air compressor	81.95	3.514	1.066	23.28	10.2	92.75	2.836	61.16	2.546	1.206	32.15	10.36	93.43	2.397
Combustion chamber	1058	32.07	0.05133	0.1598	31.11	76.3	36.6	775.2	23.1	0.03482	0.1505	25.07	79.98	30.38
Gas turbine 1	120.2	4.776	1.889	28.35	7.875	94.66	4.158	96.34	3.591	4.841	57.41	11.72	95.25	3.776
Gas heater	115.9	4.607	2.002	30.29	20.76	87.36	4.011	123.2	4.594	1.488	24.47	22.27	85.6	4.83
Gas turbine 2	95.86	5.528	2.334	29.69	15	90.46	3.317	55.93	2.829	1.417	33.36	13.17	91.93	2.192
Compressor 1	27.51	1.824	0.4871	21.07	14.43	89.78	0.9519	20.37	1.166	0.3356	22.35	14.67	89.78	0.7983
Compressor 2	26.1	1.731	0.1084	5.894	9.752	91.59	0.9031	9.336	0.5345	0.02343	4.2	10.62	90.77	0.3659
Vapor generator 1	12.73	0.734	0.0754	9.315	18.19	85.84	0.4405	51.78	2.619	0.07552	2.802	38.03	73.01	2.029
Vapor generator 2	36.54	2.258	0.1996	8.124	20.33	84.26	1.264	12.78	0.6668	0.1868	21.89	15.46	89.22	0.501
Turbine 1	18.55	1.621	0.9146	36.07	22.43	87.46	0.6417	10.33	0.8067	1.131	58.36	31.97	88.25	0.4047
Ejector	89.57	4.11	0	0	303.5	24.79	3.099	116.1	4.33	0	0	451	18.15	4.549
Condenser	1006	1.165	0.0992	7.85	17243	0.6254	34.8	1022	0.4837	0.1001	17.15	52311	0.2302	40.06
Evaporator	14.64	2.709	0.1479	5.175	84.91	55.4	0.5064	13.43	2.761	0.3122	10.16	47.43	70.12	0.5265
Pump 1	0.6309	0.06751	0.1392	67.34	34.02	90	0.02183	0.5716	0.05894	0.1295	68.73	35.63	89.97	0.0224
Pump 2	0.2285	0.02445	0.08171	76.97	36.06	92.33	0.007906	0.3974	0.04097	0.1218	74.84	32.67	92.4	0.01557
Pump 3	3.681	0.0339	0.2467	87.92	291.7	73.95	0.1274	3.726	0.02773	0.2489	89.98	351.5	73.95	0.146
Turbine 2	113.7	0.6625	0.9972	60.08	58.02	81.2	3.934	114.9	0.4917	1.01	67.25	73.87	80.52	4.503
Preheater	68.58	2.726	0.5228	16.09	469.7	20.24	2.373	63.82	2.379	0.4435	15.71	787.6	13.09	2.501
Total system	2890	70.16	11.36	13.94	63.69	38.85	-	2552	53.03	13.1	19.82	65.4	41.24	-

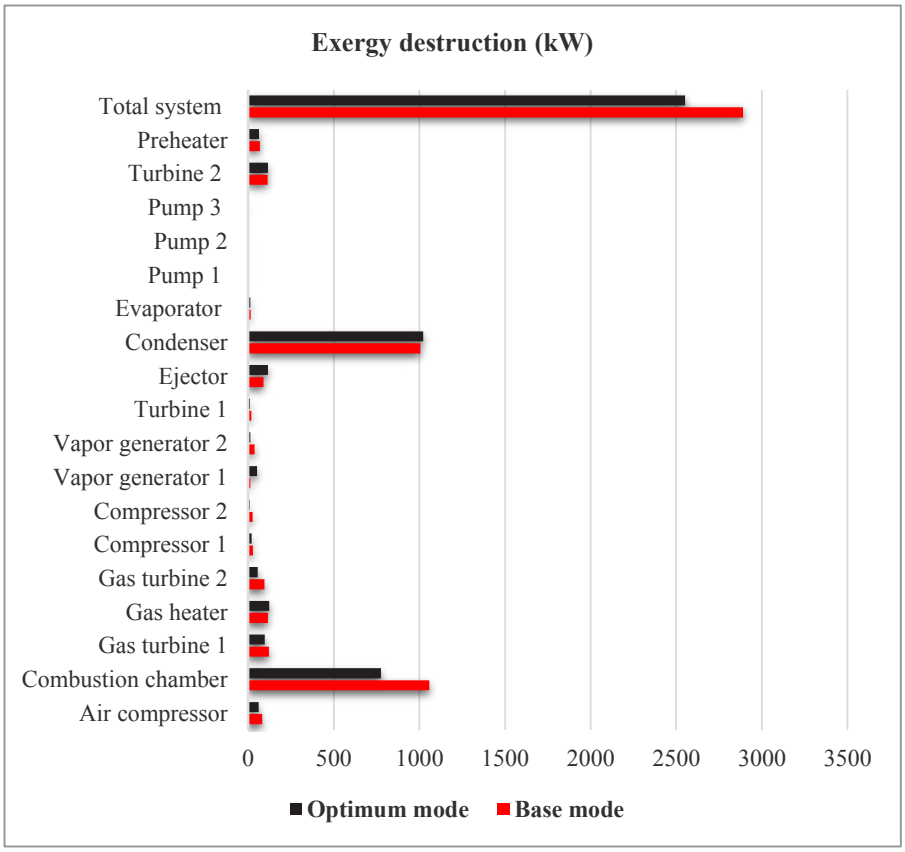

Fig. 5. Contribution of components to the exergy destruction rate at base and optimum modes.

5- 5- 1- Impact of gas turbine 1 inlet temperature

The influence of gas turbine 1 inlet temperature (GT1-IT) on the cooling load, electricity, energetic efficiency, exergetic efficiency, and UOPC of the GT cycle, CLBC cycle, and overall CCP system is sketched in Fig. 6. As GT1-IT varies in the selected range (1,200-1,600 K), a minimum point for the mass flow rate of CLBC is observed, leading to supply of heat with minimum value via vapor generators. As a result, the net produced power of the combined GT-CLBC system and cooling load will have a minimum value of 1,329.18 kW and 241.28 kW at around $T_{GT1,in}=1325(\mathrm{K})$. Similarly, the net electricity of the overall CCP system has also a minimum value of 1,913.8 kW at around $T_{GT1,in}=1540(\mathrm{K})$. The thermal load of the combustion chamber and its exergy rate are dropped more substantially than the net electricity and cooling, and hence the exergetic and energetic efficiencies of the GT cycle, CLBC cycle, and overall CCP system will go up as the GT1-IT augments. Meantime, the UOPC of the system drops as GT1-IT augments up to $T_{GT1,in}=1475(\mathrm{K})$ and increases thereafter. Moreover, the attained results also reveal that the developed cogeneration unit surpasses over the GT and CLBC systems through all GT1-IT ranges in terms of performance and cost.

5- 5- 2- Impact of methane mole fraction

The influence of methane molar fraction (MMF) on the cooling load, electricity, and energetic and exergetic efficiencies of the developed new CCP system as well as the basic GT cycle is sketched in Fig. 7. Under the same electricity attained from the GT cycle, the net power of the unit is raised up as MMF rises. Since more thermal energy is rejected to the CLBC and ORC-based CCP system via gas heaters and vapor generators. Therefore, more vapors are directed to the ejector, and hence the cooling capacity of the unit increases with the rise of MMF. Furthermore, with the rise of MMF the input thermal heat of the combustion process increases. Since the augmentation rate of output commodities (cooling and electricity) is less than that of the input heat, hence the energetic efficiency is dropped with the rise of MMF. Furthermore, the biogas exergy as well as cooling exergy rate increase as MFF increases. However, the net electricity alteration mainly influences the tendency of exergetic efficiency (due to its high value), and hence the exergetic efficiency increases as MMF augments. It can be deduced that the suggested cogeneration unit is better option instead of the basic topping system through all MMF ranges.

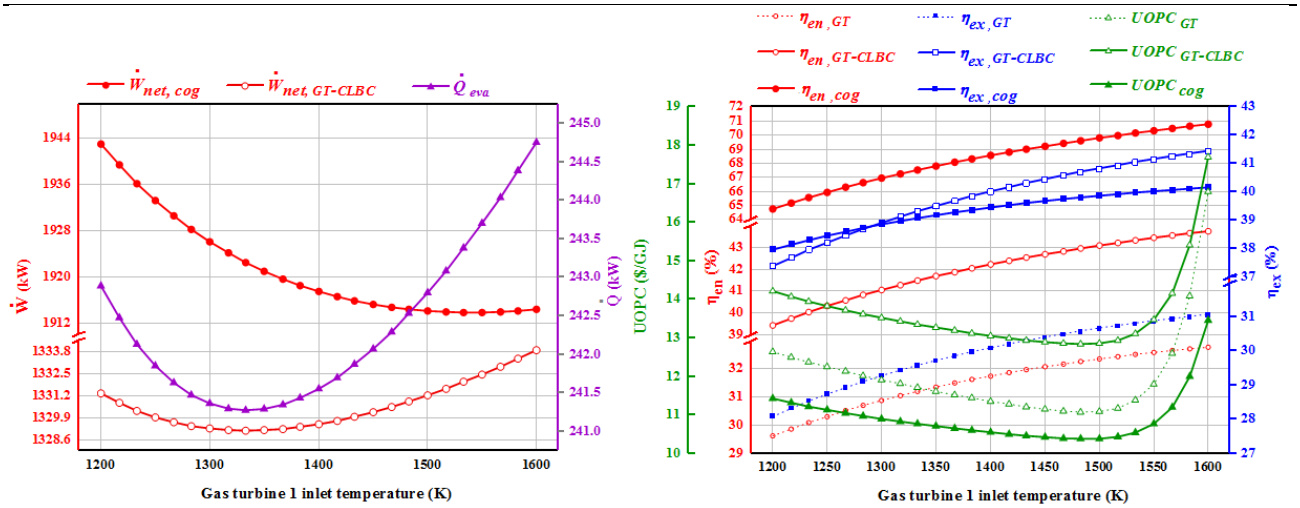

Fig. 6. Impact of GT1-IT on the: net electricity, cooling load, energetic and exergetic efficiencies, and UOPC of GT, GT-CLBC, and overall CCP systems.

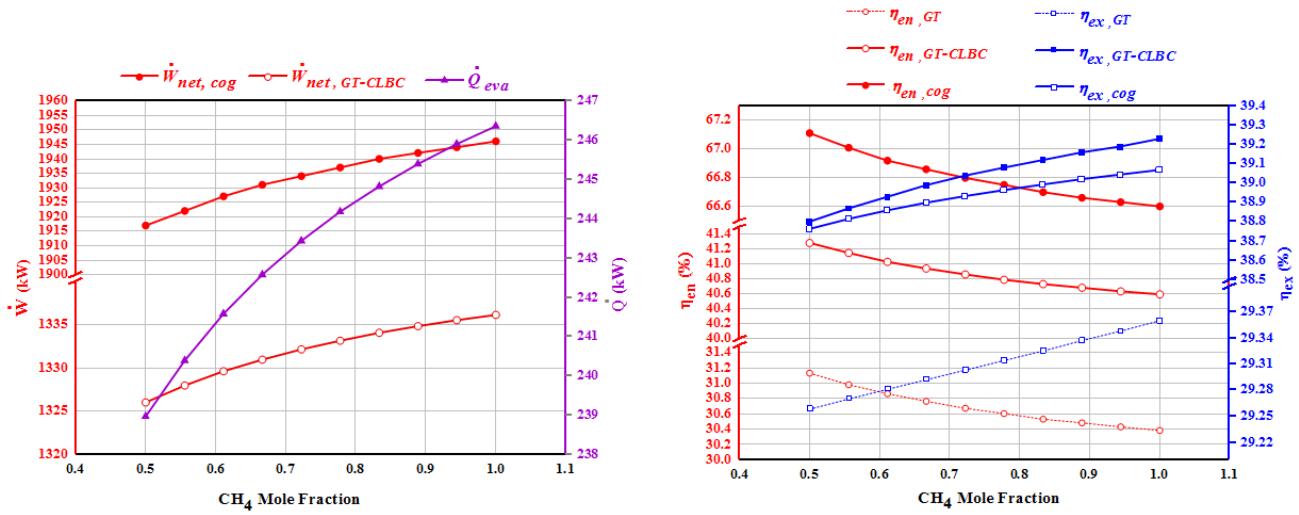

Fig. 7. Impact of MMF on the: net electricity, cooling load, and energetic and exergetic efficiencies of the GT, GT-CLBC, and overall CCP systems.

5- 5- 3- Impact of air compressor pressure ratio

Fig. 8 displays the effect of air compressor pressure ratio (ACPR) on the cooling, net electricity, energetic and exergetic efficiencies, and UOPC of the fundamental systems as well as the overall cogeneration unit. The cooling load and net electricity declines as ACPR augments, since less heat will be supplied to CLBC and ORC-based CCP systems; which led to a decrement in mass flow rate of the circulated refrigerant through these systems. By contrast, the energetic and exergetic efficiencies of the GT and CLBC systems augment as ACPR increases since decrement rate of the heat supplied by combustion process is appreciably higher than the output commodities decrement. However, due to significant decrement of the net electricity as a result of integrating of LNG power generation and ORC-based CCP systems with the GT-CLBC system, a maximum value of 66.96% is seen for the energetic efficiency of the overall cogeneration system at ACPR=11. Through this variance, the UOPC of the GT and overall CCP systems increases as ACPR augments, showing that the UOPC of the overall proposed CCP system is lower than two other systems in all ACPR ranges.

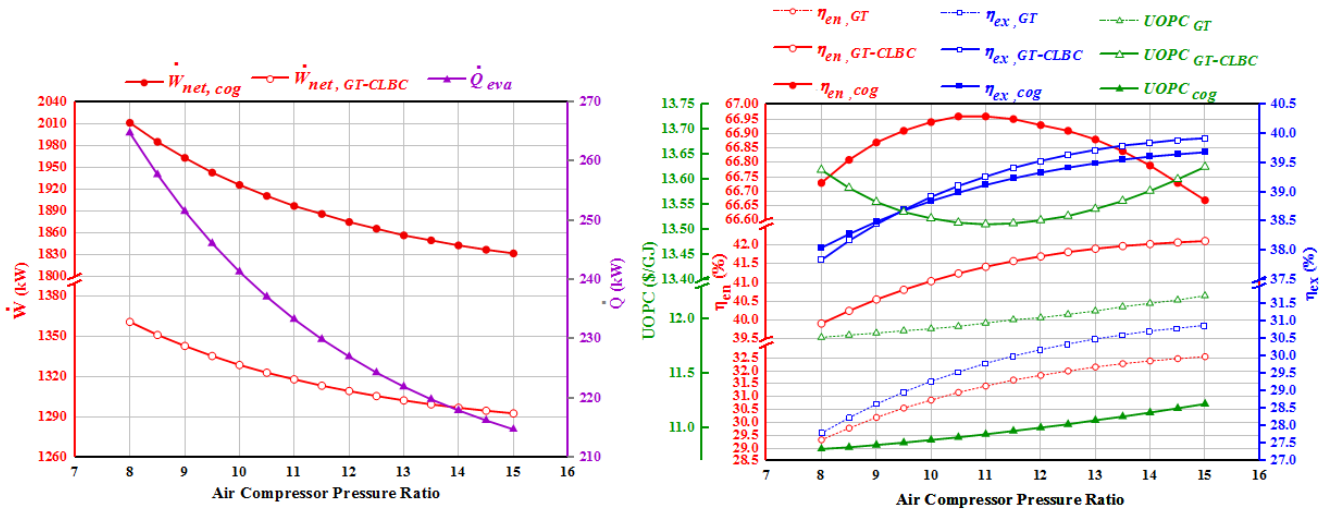

Fig. 8. Impact of ACPR on the: net electricity, cooling load, energetic and exergetic efficiencies, and UOPC of the GT, GT-CLBC, and overall CCP systems.

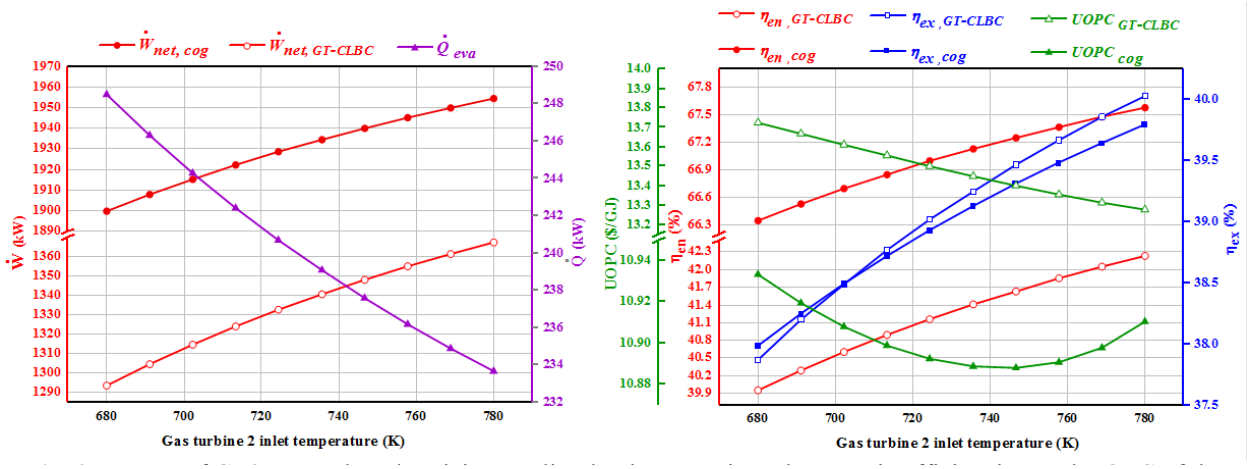

Fig. 9. Impact of GT2-IT on the: electricity, cooling load, energetic and exergetic efficiencies, and UOPC of the GT-CLBC and overall CCP systems.

5- 5- 4- Impact of gas turbine 2 inlet temperature

The influence of GT2-IT (gas turbine 2 inlet temperature) on the cooling, electricity, energetic and exergetic efficiencies and UOPC of the basic and developed CCP unit is shown in Fig. 9. As GT2-IT increases, the gas turbine 2 extracted electricity as well as compressors 1 and 2 utilized power decline. However, since decrement rate of the utilized electricity of compressors is significant than that of the extracted electricity of GT 2, the CLBC and overall CCP system electricity will aggrandize. Increasing GT2-IT also leads to increment of vapor generator 1 heat directed into the ORC-based CCP system which will result in reduction of vapor generator 2 received heating more substantially. Consequently, the mass flow rate of the saturated vapor with intermediate pressure will decline, leading to less extraction of vapor from turbine 1. Thus, the motive vapor mass flow rate will lessen, drawing less secondary flow into the ejector. Hence, increasing the gas turbine 2 inlet temperature lessens the generated cooling load. Since increment rate of net electricity outweigh decrement rate of cooling load in terms of first and second laws of thermodynamics, hence the energetic and exergetic efficiencies of both CLBC and overall systems will augment. From economic perspective, the UOPC of the CLBC system decreases as GT2-IT augments since the rate

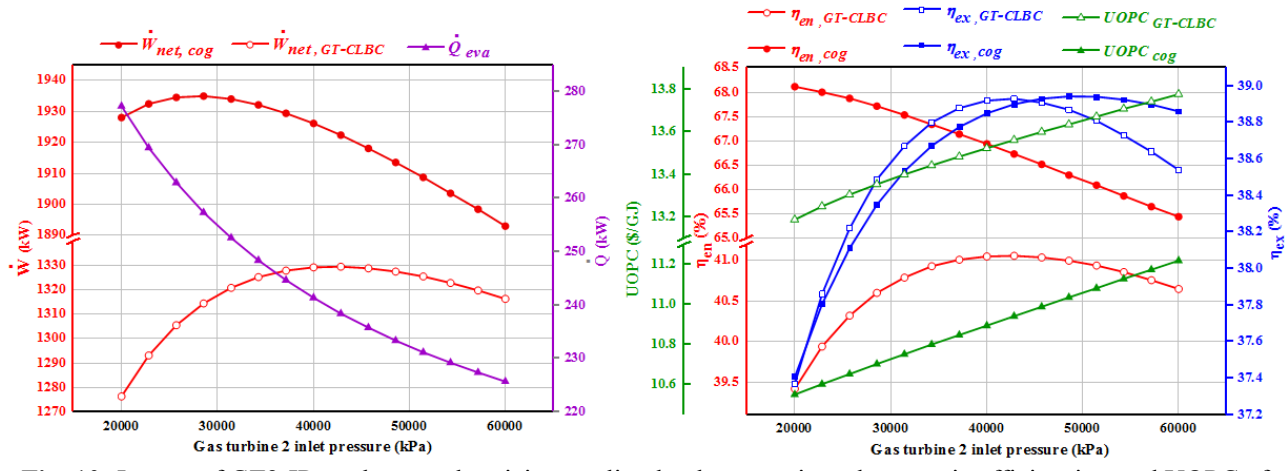

Fig. 10. Impact of GT2-IP on the: net electricity, cooling load, energetic and exergetic efficiencies, and UOPC of the GT-CLBC and overall CCP systems.

of generated electricity is considerable. However, in terms of UOPC of the overall CCP system, the rate of generated electricity is only substantial until around 746 K, while its cost rate will become more significant onward. Therefore, a nadir point is observed for the UOPC of the overall CCP system versus of GT2-IT. Moreover, based on Fig. 8 it can be deduced that the overall CCP system surpasses to the basic electricity generation systems (GT and GT-CLBC systems) through all GT2-IT ranges in terms of first law efficiency and cost.

5- 5- 5- Impact of gas turbine 2 inlet pressure

The effect of GT2-IP (gas turbine 2 inlet pressure) on the cooling load, electricity, energetic and exergetic efficiencies and UOPC of the GT-CLBC and overall CCP unit is sketched in Fig. 10. As GT2-IP increases, gas turbine 2 power and compressors utilized electricity go up. Through a precise inspection, it is discovered that the increment rate of GT 2 output electricity is substantial than that of the compressors utilized electricity up to $P_{GT\,2,in} = 42857(\text{kPa})$, while the trend is reverted onward. The fact is also true concerning the overall net electricity, where the maximum net overall electricity is observed at $P_{GT\,2,in} = 28571(\text{kPa})$. The maximunm combined GT-CLBC and overall CCP systems are computed at 1,329.57 kW and 1,934.94 kW, respectively. Due to the same reason pinpointed in the previous sub-section, the cooling load declines as GT2-IP augments. From thermodynamics vantage point, the variation trend of energetic efficiency of the GT-CLBC system is similar to its net electricity since generated net electricity has a dominant impact on thermal performance. In overall CCP system, the variation trend of energetic efficiency of the overall CCP system is nearly similar to its net electricity except the fact that the peak value is not observed in the examined range. In terms of exergy, a peak value is seen for exergetic efficiencies of both combined GT-CLBC and overall CCP systems at approximately $P_{GT\,2,in} = 42857(\text{kPa})$ and $P_{GT\,2,in} = 48571(\text{kPa})$, respectively. At this condition, the maximum exergetic efficiencies of the combined GT-CLBC and overall CCP systems are computed at 38.92% and 38.94%, respectively. From economic standpoint, the UOPC of the GT-CLBC and overall CCP systems increases as the cost rate of electricity generated by turbines increases continuously.

5- 5- 6- Impact of gas turbine 2 outlet pressure

The impact of GT2-OP (gas turbine 2 outlet pressure) on the cooling load, electricity, energetic and exergetic efficiencies, and UOPC of the GT-CLBC and overall CCP systems is sketched in Fig. 11. As GT2-OP increases, the gas turbine 2 extracted electricity as well as compressors 1 and 2 utilized power go down. However, since decrement rate of the utilized electricity of compressors is significant than that of the extracted electricity of GT 2, the CLBC and overall CCP system electricity will aggrandize. Increasing GT2-OP also leads to increment of vapor generator 1 heat directed into the ORC-based CCP system which will result in reduction of vapor generator 2 received heating more substantially. Consequently, the mass flow rate of the saturated vapor with intermediate pressure will decline, leading to less extraction of vapor from turbine 1. Thus, the motive vapor mass flow rate will lessen, drawing less secondary flow into the ejector. Hence, increasing the gas turbine 2 outlet pressure has a same effect as the gas turbine 2 inlet temperature and will lessen the generated cooling load. Since the increment rate of net electricity outweighs decrement rate of cooling load in terms of first and second laws of thermodynamics, hence the energetic and exergetic efficiencies of both CLBC and overall systems will augment. From economic perspective, the UOPC of the CLBC system has a peak value of 13.52

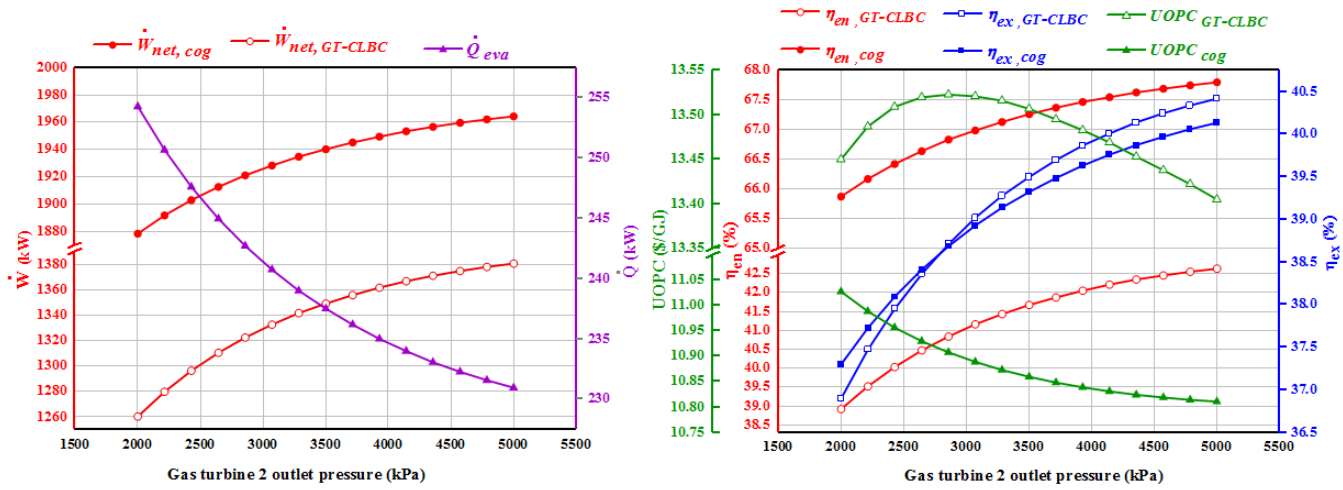

Fig. 11. Impact of GT2-OP on the: net electricity, cooling load, energetic and exergetic efficiencies, and UOPC of the GT-CLBC and overall CCP systems.

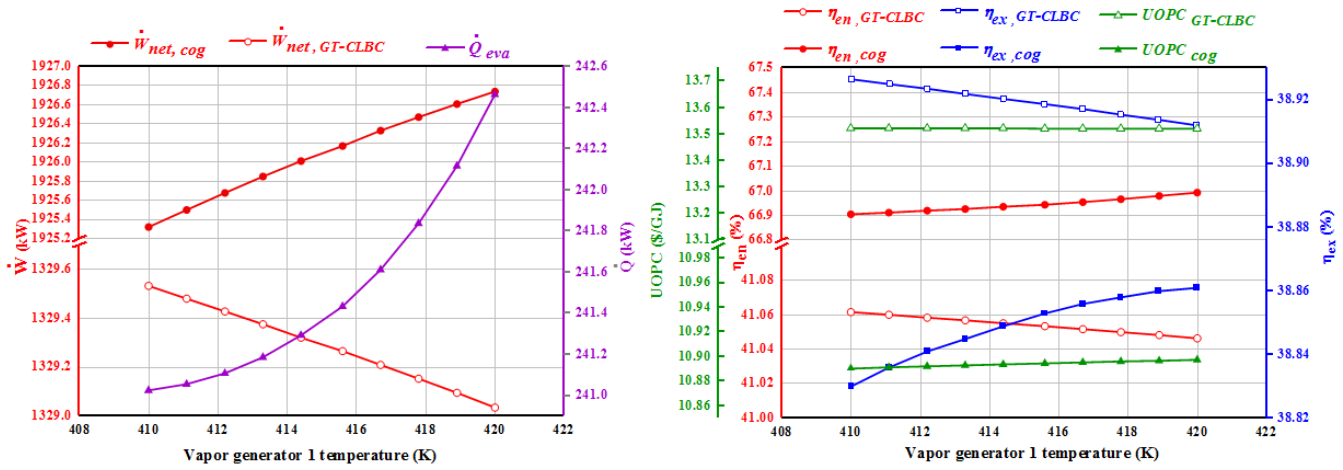

Fig. 12. Impact of VG1 temperature on the: electricity, cooling load, energetic and exergetic efficiencies, and UOPC of the GT-CLBC and overall CCP systems.

$/GJ at GT2-OP of 2,857 kPa. Meantime, the UOPC of the overall CCP system reduces as the GT2-OP increases due to a large value of net overall electricity and its dominant impact.

5- 5- 7- Impact of vapor generator 1 temperature

Fig. 12 exhibits the impact of VG1-T (vapor generator 1 temperature) on the electricity, cooling load, energetic and exergetic efficiencies, and UOPC of the GT-CLBC and overall CCP systems. As the VG1-T augments, electricity generated by the GT-CLBC system decrease so subtly since inlet energy of compressor 1 is aggrandized slightly and compressor 1 utilized power augments. On the other side, generate electricity via turbine 1 is raised as vapor generator 1 temperature goes up, and hence the net electricity of overall CCP system will increase. This variation also increases suction power of ejector through the throat nozzle and hence cooling load will aggrandize as well. Variation of energetic and exergetic efficiencies of both combined GT-CLBC and overall CCP systems with vapor generator 1 temperature resembles the variation of electricity as expounded earlier, since energetic efficiency is only affected by output commodities and input heat via combustion process is unvaried. As vapor generator 1 temperature augments, the net electricity and cooling load increased, too; which leads to increment of cost rate associate with these commodities with a same order. Thus, an exact inspection reveals that the UOPC of both combined GT-CLBC and overall CCP system will remained nearly fixed with any alteration in the vapor

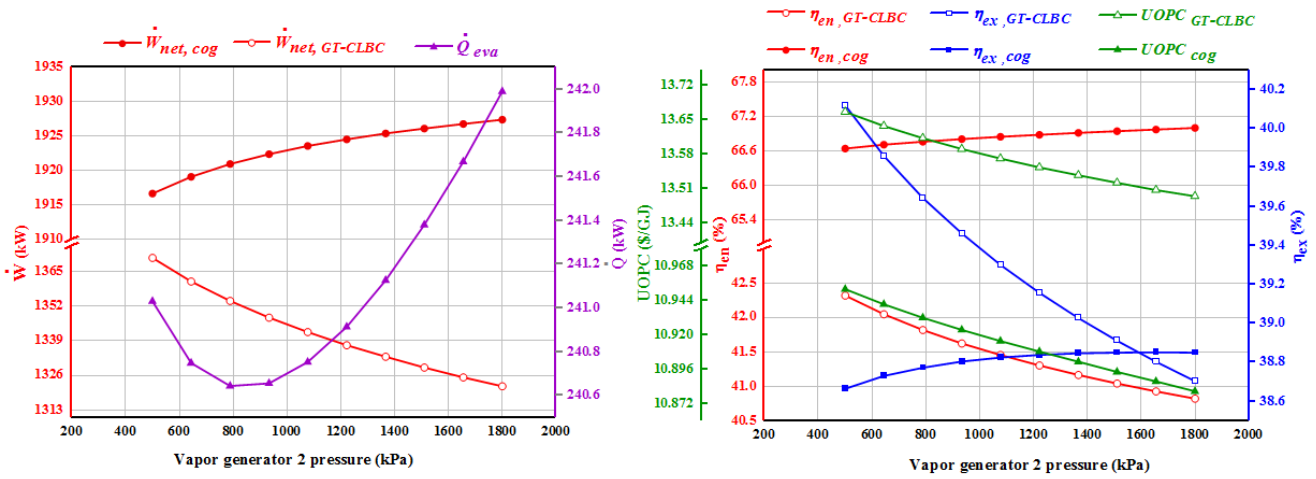

Fig. 13. Impact of VG2 pressure on the: electricity, cooling load, energetic and exergetic efficiencies, and UOPC of the GT-CLBC and overall CCP systems.

generator 1 temperature.

5- 5- 8- Impact of vapor generator 2 pressure

Fig. 13 exhibits the impact of vapor generator 2 pressure (VG2-P) on the cooling load, electricity, energetic and exergetic efficiencies, and UOPC of the GT-CLBC and overall CCP systems. As the VG2-P augments, electricity generated by the GT-CLBC system decreases since inlet and outlet energies of compressor 2 are aggrandized, and more utilized will be used by compressors. Even though other expansion/compression components influence the electricity variation of the GT-CLBC system, but their impacts are negligible versus the compressor 1 consumption electricity increment. Additionally, as vapor generator 2 pressure goes up, more electricity will be generated via turbine 1 and hence the net electricity of the overall CCP system will increase. This variation also increases suction power of the ejector through the throat nozzle at high vapor generator 2 pressures (only at >790 kPa), while will decrease suction power at low pressures. Hence, the cooling load will have a minimum point versus of the VG2-P. Variation of energetic and exergetic efficiencies of both combined GT-CLBC and overall CCP systems with vapor generator 2 pressure resembles the variation of electricity (similar to vapor generator 1 temperature), since energetic and exergetic efficiencies are only affected by output commodities. Thus, the energetic and exergetic efficiencies of the combined GT-CLBC system lessens as vapor generator 2 pressure augments, whilst the energetic and exergetic efficiencies of the overall CCP system augments throughout this alteration. A precise inspection reveals that the UOPC of both combined GT-CLBC and overall CCP systems goes down as the vapor generator 2 pressure augments.

5- 5- 9- Impact of condenser pressure

Fig. 14 shows the variation of the cooling load, electricity, energetic and exergetic efficiencies, and UOPC of the combined GT-CLBC and overall CCP systems with disparate condenser pressures. With the rise of the condenser pressure no changes occur in the topping sub-cycle, and hence the changes are observed at the bottoming sub-cycle (ORC-based CCP system). According to this sketch, increasing condenser pressure decreases cooling load (since the inlet energy of evaporator augments), while increasing the electricity extracted from the combined GT-CLBC and overall CCP systems. The central reasons are as follows. As condenser pressure augments, turbine 1 electricity increases, whilst utilized power of compressor 1 declines. Even though capacities of other expansion/compression equipment vary, but these two components play a significant role in evaluation. From second law of thermodynamics perspective, net electricity of each examined system will influence exergetic efficiency of the systems as condenser pressure varies. Accordingly, increasing condenser temperature raises the exergetic efficiency of both combined systems due to net electricity increment rate. In terms of 1st law of thermodynamics, the energetic efficiency of the combined GT-CLBC system increases as condenser pressure increases, since its net electricity is raised. However, the energetic efficiency of the overall CCP system has a minimum decrease at low condenser pressures, while increases at high condenser pressures. This is critically because, at low condensation pressures decrement of cooling load is substantial than increment of electricity, whilst the trend is reverse at high condenser pressures. In terms of economic evaluation of systems, the UOPC of the combined GT-CLBC system goes up so slightly (since the generated electricity in this system

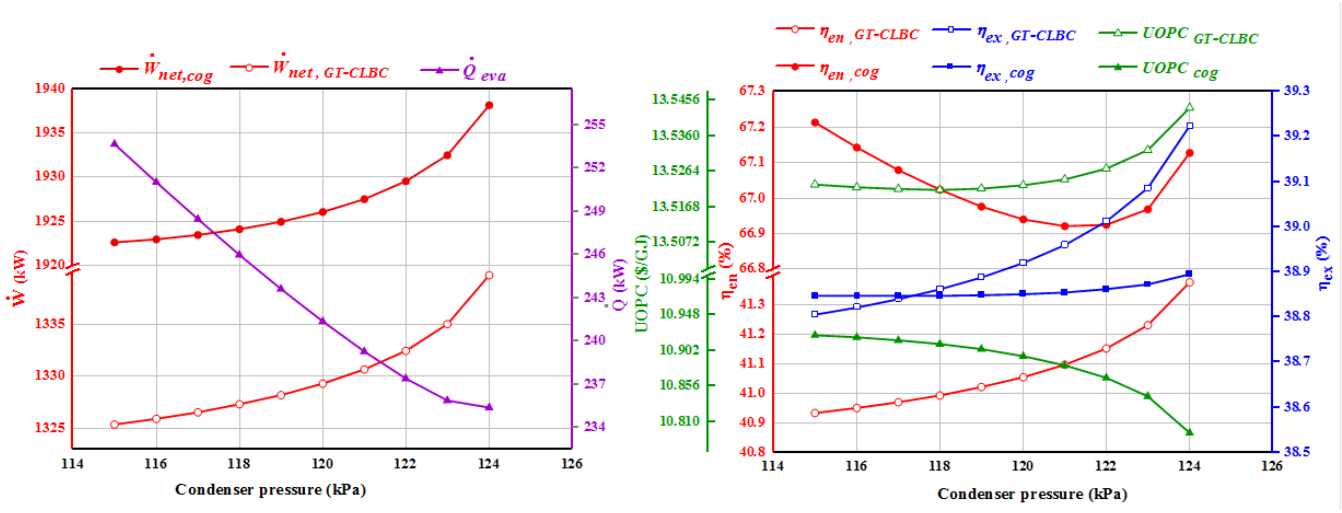

Fig. 14. Impact of condenser pressure on the: electricity, cooling load, energetic and exergetic efficiencies, and UOPC of the GT-CLBC and overall CCP systems.

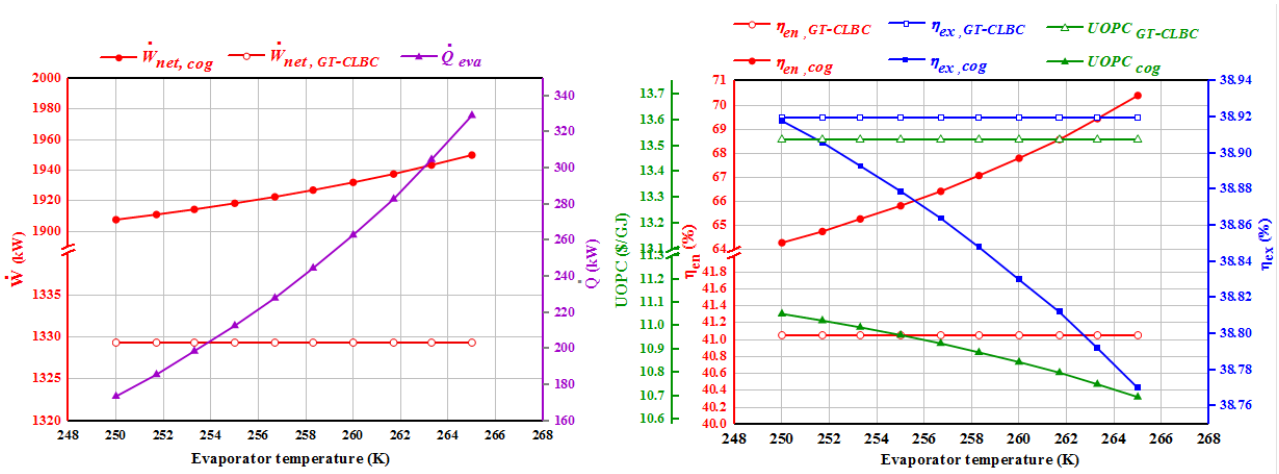

Fig. 15. Impact of evaporator temperature on the: electricity, cooling load, energetic and exergetic efficiencies, and UOPC of the GT-CLBC and overall CCP systems.

and the cost rate associated with it increase with the same dominance), while the UOPC of the overall CCP system is decreased (since the generated electricity in this system rises appreciably).

5- 5- 10- Impact of evaporator temperature

Fig. 15 shows variance of the cooling load, electricity, energetic and exergetic efficiencies and UOPC of the combined GT-CLBC and overall CCP systems with disparate evaporator temperatures. The net electricity and cooling load of the overall CCP system augment as evaporator temperature augments, while electricity of the combined GT-CLBC system remaines constant. As a result, the energetic and exergetic efficiencies and UOPC of the combined GT-CLBC system will remain unvaried. However, the energetic efficiency of the overall CCP system increases as evaporation temperature aggrandizes (since cooling load and net electricity increase), while its exergetic efficiency declines since the exergy of LNG supplied to the overall system goes up substantially. The UOPC of the overall CCP system also reduces as evaporator temperature augments mainly due to the considerable increment of net electricity in comparison with its cost rate.

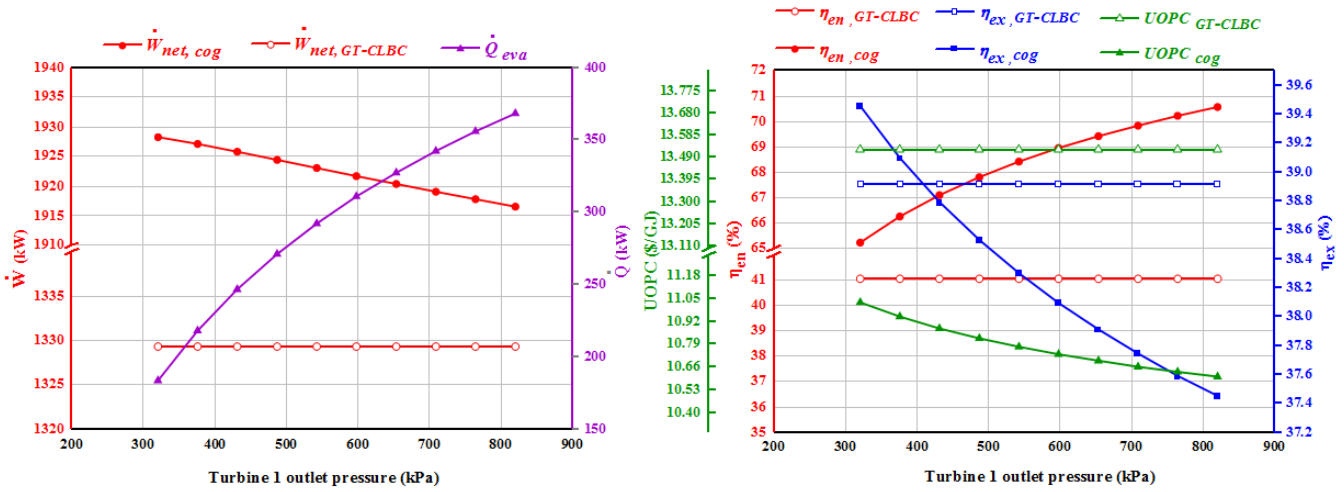

Fig. 16. Impact of turbine 1 outlet pressure on the: electricity, cooling load, energetic and exergetic efficiencies, and UOPC of the GT-CLBC and overall CCP systems.

5- 5- 11- Impact of turbine 1 outlet pressure

Fig. 16 portrays variance of the electricity, cooling load, energetic and exergetic efficiencies and UOPC of the combined GT-CLBC and overall CCP systems with disparate turbine 1 outlet pressures (T1-OPs). The cooling load of the overall CCP system augments as turbine 1 outlet pressure augments, whilst its net electricity decreases since turbine 1 expansion ration decreases. Since increment rate of cooling load is appreciable than decrement rate of net electricity, thus the energetic efficiency of the overall CCP system will augment. In contrary, since increment rate of exergy of cooling is insignificant than the decrement rate of net electricity, thus the exergetic efficiency and UOPC of the overall CCP system will lessen. However, electricity of the combined GT-CLBC system remaines constant, and consequently the energetic and exergetic efficiencies and UOPC of the combined GT-CLBC system will remain unvaried.

6- Conclusions

This study aimed to propose a new waste heat recovery process for a biogas-fueled gas turbine (GT) cycle using three efficient stages. These stages include a close loop Brayton cycle (CLBC), a liquefied natural gas (LNG) open power generation cycle, and a dual-stage combined cooling and power (CCP) unit composed of an organic Rankine cycle (ORC) integrated with an ejector refrigeration cycle (ERC). Thermodynamic and economic analyses were performed and a multi-objective optimization was applied to the calculations through a genetic algorithm. The main findings are as below:

Among all elements, the major device in terms of irreversibility was the combustion chamber, which had the highest exergy destruction rate, followed by the condenser (first heat recovery from liquefied natural gas).

The base case designated the net output electricity and cooling at 1926 kW and 241.4 kW, respectively. Additionally, the energy efficiency, exergy efficiency, and UOPC were calculated at 66.94%, 38.85%, and 10.89 $/GJ, respectively.

The multi-objective optimization improved the energy efficiency by 20.1%, the exergy efficiency by 6.15%, and the UOPC by 7.52%. In this way, the cooling load increased by 75.68%, whilst the net electricity decreased by 3.21%. The optimum cooling load, net electricity, energy and exergy efficiencies, and UOPC of the suggested system were calculated at 424.1 kW, 1,864 kW, 80.4%, 41.24%, 10.07 $/GJ, respectively.

In the optimum mode, the energy and exergy efficiencies of the GT cycle were improved by 33.66% and 33.68%, respectively, as CLBC cycle was employed.

The combined GT-CLBC system had approximately 13.51% higher unit cost (in the base mode) than the GT cycle.

In the optimum mode, the energy and exergy efficiencies of the overall CCP system were improved by 71.17% and exergy efficiency declined by 7.38% (compared to the as combined GT-CLBC system). From economic vantage point, the UOPC of the integrated CCP system was declined by 19.45% (in the base mode) and 20.45% (in the optimum mode), compared to the GT-CLBC system.

This study increased the energy and exergy efficiency and decreased the products' unit cost compared to similar work. Considering the economic comparison, a reduction of 23% was achievable. So, this system is practically and economically justifiable.

From the economic point of view, the total investment cost rate and exergy destruction cost rate of the system at the optimum mode were computed at 13.1 $/h and 53.03 $/h leading to the overall exergoeconomic factor and relative cost difference of 19.82% and 65.4%, respectively. These values were 5.88% and 1.71% better than the base case.

Generally, GT 1 inlet temperature imposed the highest sensitivity to the overall performance of the system. In detail, the highest sensitivity index of the exergy efficiency at 0.534, the second-highest sensitivity index of the energy efficiency at 0.243, and the second-highest sensitivity index of the UOPC at 0.173 belong to this decision variable. In addition, the highest sensitivity index of the energy efficiency and UOPC belongs to the evaporator temperature and GT 2 outlet pressure at 0.246 and 0.223, respectively.

Nomenclature

Symbols

A	Area (m^2)
AC	Air compressor
ACPR	AC pressure ratio
c	Cost per unit exergy ($\$.GJ^{-1}$)
$\dot{C}$	Cost rate ($\$.yr^{-1}$)
CC	Combustion chamber
CCP	Combined cooling and power
CLBC	Close loop Brayton cycle
CRF	Capital recovery factor
ERC	Ejector refrigeration cycle
ex	Exergy per unit mass ($kW.kg^{-1}$)
$\overline{ex}_i^{ch,0}$	Standard chemical exergy of stream i ($kW.kg^{-1}$)
$\dot{E}x$	Exergy rate (kW)
f_k	Exergoeconomic factor
FP	Fuel price ($/GJ)
GA	Genetic algorithm
GH	Gas heater
GT	Gas turbine
h	Specific enthalpy ($kJ.kg^{-1}$)
IP	İnlet pressure
k_i	Interest rate
LHV	Lower heating value
LNG	Liquefied natural gas
$\dot{m}$	Mass flow rate ($kg.s^{-1}$)
MMF	methane molar fraction
MOO	Multi-objective operator
$\dot{n}$	Molar rate ($kmol.s^{-1}$)
N	Annual number of hours (h)
n_r	Componets expected lifetime
OP	Outlet pressure
OT	Outlet temperature
ORC	Organic Rankine cycle
P	Pressure (bar)
PH	Preheater
R	Universial gases constant ($J.kg^{-1}.K^{-1}$)
r_{AC}	AC pressure ratio
r_k	Relative cost difference
s	Specific entropy ($kJ.kg^{-1}.K^{-1}$)
T	Temperature (℃)
TTD	Terminal temperature difference (K)
ΔT_{LMTD}	Logaritmic mean temperture difference
U	Overall heat transfer coefficient ($kW.m^{-2}K^{-1}$)
UOPC	Unit overall product cost ($/GJ)
u	Velocity (m/s)
$\dot{W}$	Power or Electricity (kW)
w	Weigh coefficient
y_D	Exergy destruction ratio (%)
y_i	Molar fraction of stream i
Z	Investment cost of components ($)
$\dot{Z}$	İnvestment cost rate of components ($\$.yr^{-1}$)

Greek Symbols

β	Turbine expansion ratio
η	Efficiency (%)
ϕ_r	Maintenance factor
λ	Fuel/air ratio
μ	Mass entrainment ratio

Subscripts and superscripts

AC	Air compressor
cc	Combustion chamber
ch	Chemical
CI	capital investment
cog	Cogeneration
cond	Condenser
comp	Compressor
c.v.	Control volume
D	Destruction
d	Diffuser
en	Energetic
eva	Evaporator
ex	Exergetic
F	Fuel
in	İnlet
is	İsentropic
i	i^{th} strream
LMTD	Logarithmic mean temperature difference
m	Mixer
mf	Mixed fluid
n	Nozzle
net	Net value
OM	Operating & maintenance
out	Outlet
P	Product
pf	Primary fluid
ph	Physical
pp	Pinch point
pu	Pump
q	Heat transfer
s	Constant entropy
sf	Secondary fluid
tur	Turbine
vg	Vapor generator
w	Water
1, 2, …	Cycle locations
0	Dead state

References

[1] H. Ghaebi, M. Yari, S.G. Gargari, H. Rostamzadeh, Thermodynamic modeling and optimization of a combined biogas steam reforming system and organic Rankine cycle for coproduction of power and hydrogen, Renewable Energy, (2018).

[2] A.D. Zareh, R.K. Saray, S. Mirmasoumi, K. Bahlouli, Extensive thermodynamic and economic analysis of the cogeneration of heat and power system fueled by the blend of natural gas and biogas, Energy Conversion and Management, 164 (2018) 329-343.

[3] S. Amiri, D. Henning, B.G. Karlsson, Simulation and introduction of a CHP plant in a Swedish biogas system, Renewable energy, 49 (2013) 242-249.

[4] H. Zeng, Y. Wang, Y. Shi, N. Cai, Biogas-fueled flame fuel cell for micro-combined heat and power system, Energy Conversion and Management, 148 (2017) 701-707.

[5] F. Jabari, B. Mohammadi-ivatloo, M.-B. Bannae-Sharifian, H. Ghaebi, Design and performance investigation of a biogas fueled combined cooling and power generation system, Energy Conversion and Management, 169 (2018) 371-382.

[6] G. Leonzio, An innovative trigeneration system using biogas as renewable energy, Chinese Journal of Chemical Engineering, 26(5) (2018) 1179-1191.

[7] E. Sevinchan, I. Dincer, H. Lang, Energy and exergy analyses of a biogas driven multigenerational system, Energy, 166 (2019) 715-723.

[8] H. Rostamzadeh, S.G. Gargari, A.S. Namin, H. Ghaebi, A novel multigeneration system driven by a hybrid biogas-geothermal heat source, Part I: Thermodynamic modeling, Energy Conversion and Management, 177 (2018) 535-562.

[9] H. Rostamzadeh, S.G. Gargari, A.S. Namin, H. Ghaebi, A novel multigeneration system driven by a hybrid biogas-geothermal heat source, Part II: Multi-criteria optimization, Energy Conversion and Management, 180 (2018) 859-888.

[10] B. Su, W. Han, Y. Chen, Z. Wang, W. Qu, H. Jin, Performance optimization of a solar assisted CCHP based on biogas reforming, Energy Conversion and Management, 171 (2018) 604-617.

[11] Y. Liang, J. Chen, X. Luo, J. Chen, Z. Yang, Y. Chen, Simultaneous optimization of combined supercritical CO2 Brayton cycle and organic Rankine cycle integrated with concentrated solar power system, Journal of Cleaner Production, 266 (2020) 121927.

[12] G.V. Ochoa, J.D. Forero, J.P. Rojas, A comparative energy and exergy optimization of a supercritical-CO2 Brayton cycle and Organic Rankine Cycle combined system using swarm intelligence algorithms, Heliyon, 6(6) (2020) e04136.

[13] Y. Yang, Y. Huang, P. Jiang, Y. Zhu, Multi-objective optimization of combined cooling, heating, and power systems with supercritical CO2 recompression Brayton cycle, Applied Energy, 271 (2020) 115189.

[14] T. Gholizadeh, M. Vajdi, F. Mohammadkhani, Thermodynamic and thermoeconomic analysis of basic and modified power generation systems fueled by biogas, Energy conversion and management, 181 (2019) 463-475.

[15] T. Gholizadeh, M. Vajdi, H. Rostamzadeh, A new biogas-fueled bi-evaporator electricity/cooling cogeneration system: exergoeconomic optimization, Energy Conversion and Management, 196 (2019) 1193-1207.

[16] T. Gholizadeh, M. Vajdi, H. Rostamzadeh, Exergoeconomic optimization of a new trigeneration system driven by biogas for power, cooling, and freshwater production, Energy Conversion and Management, 205 (2020) 112417.

[17] S.E. Hosseini, H. Barzegaravval, M.A. Wahid, A. Ganjehkaviri, M.M. Sies, Thermodynamic assessment of integrated biogas-based micro-power generation system, Energy Conversion and Management, 128 (2016) 104-119.

[18] M. Khaljani, R.K. Saray, K. Bahlouli, Comprehensive analysis of energy, exergy and exergo-economic of cogeneration of heat and power in a combined gas turbine and organic Rankine cycle, Energy Conversion and Management, 97 (2015) 154-165.

[19] F. Javanfam, H. Ghiasirad, R. Khoshbakhti Saray, Efficiency Improvement and Cost Analysis of a New Combined Absorption Cooling and Power System, in: Synergy Development in Renewables Assisted Multi-carrier Systems, Springer, 2022, pp. 23-50.

[20] A. Farajollahi, M. Rostami, M. Feili, H. Ghaebi, Thermodynamic and economic evaluation and optimization of the applicability of integrating an innovative multi-heat recovery with a dual-flash binary geothermal power plant, Clean Technologies and Environmental Policy, (2023) 1-26.

[21] A. Farajollahi, M. Rostami, M. Feili, H. Ghaebi, M.R. Salimi, Modified cost analysis integrated with dual parametric sensitivity study for realistic cost assessment of a novel modified geothermal-based multi-generation energy system, Energy Reports, 8 (2022) 13463-13483.

[22] M. Feili, M. Hasanzadeh, H. Ghaebi, E. Abdi Aghdam, Comprehensive analysis of a novel cooling/electricity cogeneration system driven by waste heat of a marine diesel engine, Energy Sources, Part A: Recovery, Utilization, and Environmental Effects, 44(3) (2022) 7331-7346.

[23] M. Feili, H. Rostamzadeh, T. Parikhani, H. Ghaebi, Hydrogen extraction from a new integrated trigeneration system working with zeotropic mixture, using waste heat of a marine diesel engine, International Journal of Hydrogen Energy, 45(41) (2020) 21969-21994.

[24] M. Feili, H. Rostamzadeh, H. Ghaebi, Thermo-mechanical energy level approach integrated with exergoeconomic optimization for realistic cost evaluation of a novel micro-CCHP system, Renewable Energy, 190 (2022) 630-657.

[25] A. Bejan, G. Tsatsaronis, Thermal design and optimization, John Wiley & Sons, 1996.

[26] J. Szargut, D.R. Morris, F.R. Steward, Exergy analysis of thermal, chemical, and metallurgical processes, (1987).

[27] H. Ghiasirad, H. Rostamzadeh, S. Nasri, Design and evaluation of a new solar tower-based multi-generation system: Part I, thermal modeling, in: Integration of Clean and Sustainable Energy Resources and Storage in Multi-Generation Systems, Springer, 2020, pp. 83-102.

[28] H. Ghiasirad, H. Rostamzadeh, S. Nasri, Design and evaluation of a new solar tower-based multi-generation system: Part II, Exergy and exergoeconomic modeling, in: Integration of Clean and Sustainable Energy Resources and Storage in Multi-Generation Systems, Springer, 2020, pp. 103-120.

[29] H. Ghaebi, T. Parikhani, H. Rostamzadeh, Energy, exergy and thermoeconomic analysis of a novel combined cooling and power system using low-temperature heat source and LNG cold energy recovery, Energy Conversion and Management, 150 (2017) 678-692.

[30] H. Barzegaravval, S.E. Hosseini, M.A. Wahid, A. Saat, Effects of fuel composition on the economic performance of biogas-based power generation systems, Applied Thermal Engineering, 128 (2018) 1543-1554.

[31] M. Feili, H. Ghaebi, T. Parikhani, H. Rostamzadeh, Exergoeconomic analysis and optimization of a new combined power and freshwater system driven by waste heat of a marine diesel engine, Thermal Science and Engineering Progress, 18 (2020) 100513.

[32] H.N. Somehsaraei, M.M. Majoumerd, P. Breuhaus, M. Assadi, Performance analysis of a biogas-fueled micro gas turbine using a validated thermodynamic model, Applied Thermal Engineering, 66(1-2) (2014) 181-190.

[33] B. Huang, J. Chang, C. Wang, V. Petrenko, A 1-D analysis of ejector performance, International journal of refrigeration, 22(5) (1999) 354-364.

HOW TO CITE THIS ARTICLE

A. Farajollahi, M. Rostami, M.R. Salimi, F. Behnam, A modified biogas-driven combined cooling and power system based on open and close Brayton cycles, AUT J. Mech Eng., 7(2) (2023) 91-116.

DOI: 10.22060/ajme.2023.21259.6031